NUREG/CR–4667
ANL–95/2
Vol. 19

Environmentally Assisted Cracking in Light Water Reactors

Semiannual Report
April – September 1994

Manuscript Completed: August 1995
Date Published: September 1995

Prepared by
O. K. Chopra, H. M. Chung, D. J. Gavenda, E. E. Gruber, A. G. Hins,
T. H. Hughes, T. F. Kassner, W. E. Ruther, W. J. Shack, and W. K. Soppet

Argonne National Laboratory
9700 South Cass Avenue
Argonne, IL 60439

M. McNeil, NRC Project Manager

Prepared for
Division of Engineering
Office of Nuclear Regulatory Research
U.S. Nuclear Regulatory Commission
Washington, DC 20555–0001
NRC Job Code A2212

Previous Documents in Series

Environmentally Assisted Cracking in Light Water Reactors Semiannual Report April—September 1985, NUREG/CR-4667 Vol. I, ANL-86-31 (June 1986).

Environmentally Assisted Cracking in Light Water Reactors Semiannual Report October 1985—March 1986, NUREG/CR-4667 Vol. II, ANL-86-37 (September 1987).

Environmentally Assisted Cracking in Light Water Reactors Semiannual Report April—September 1986, NUREG/CR-4667 Vol. III, ANL-87-37 (September 1987).

Environmentally Assisted Cracking in Light Water Reactors Semiannual Report October 1986—March 1987, NUREG/CR-4667 Vol. IV, ANL-87-41 (December 1987).

Environmentally Assisted Cracking in Light Water Reactors Semiannual Report April—September 1987, NUREG/CR-4667 Vol. V, ANL-88-32 (June 1988).

Environmentally Assisted Cracking in Light Water Reactors Semiannual Report October 1987—March 1988, NUREG/CR-4667 Vol. 6, ANL-89/10 (August 1989).

Environmentally Assisted Cracking in Light Water Reactors Semiannual Report April—September 1988, NUREG/CR-4667 Vol. 7, ANL-89/40 (March 1990).

Environmentally Assisted Cracking in Light Water Reactors Semiannual Report October 1988—March 1989, NUREG/CR-4667 Vol. 8, ANL-90/4 (June 1990).

Environmentally Assisted Cracking in Light Water Reactors Semiannual Report April—September 1989, NUREG/CR-4667 Vol. 9, ANL-90/48 (March 1991).

Environmentally Assisted Cracking in Light Water Reactors Semiannual Report October 1989—March 1990, NUREG/CR-4667 Vol. 10, ANL-91/5 (March 1991).

Environmentally Assisted Cracking in Light Water Reactors Semiannual Report April—September 1990, NUREG/CR-4667 Vol. 11, ANL-91/9 (May 1991).

Environmentally Assisted Cracking in Light Water Reactors Semiannual Report October 1990—March 1991, NUREG/CR-4667 Vol. 12, ANL-91/24 (August 1991).

Environmentally Assisted Cracking in Light Water Reactors Semiannual Report April—September 1991, NUREG/CR-4667 Vol. 13, ANL-92/6 (March 1992).

Environmentally Assisted Cracking in Light Water Reactors Semiannual Report October 1991—March 1992, NUREG/CR-4667 Vol. 14, ANL-92/30 (August 1992).

Environmentally Assisted Cracking in Light Water Reactors Semiannual Report April—September 1992, NUREG/CR-4667 Vol. 15, ANL-93/2 (June 1993).

Environmentally Assisted Cracking in Light Water Reactors Semiannual Report October 1992—March 1993, NUREG/CR-4667 Vol. 16, ANL-93/27 (September 1993).

Environmentally Assisted Cracking in Light Water Reactors Semiannual Report April—September 1993, NUREG/CR-4667 Vol. 17, ANL-94/26 (June 1994).

Environmentally Assisted Cracking in Light Water Reactors Semiannual Report October 1993—March 1994, NUREG/CR-4667 Vol. 18, ANL-95/2 (March 1995).

Environmentally Assisted Cracking in Light Water Reactors Semiannual Report April 1994–September 1994

by

O. K. Chopra, H. M. Chung, D. J. Gavenda, E. E. Gruber, A. G. Hins,
T. H. Hughes, T. F. Kassner, W. E. Ruther, W. J. Shack, and W. K. Soppet

Abstract

This report summarizes work performed by Argonne National Laboratory (ANL) on fatigue and environmentally assisted cracking (EAC) in light water reactors from April to September 1994. Topics that have been investigated include (a) fatigue of carbon and low–alloy steel used in piping and reactor pressure vessels, (b) EAC of austenitic stainless steels (SSs) and Alloy 600, and (c) irradiation–assisted stress corrosion cracking (IASCC) of Type 304 SS. Fatigue tests have been conducted on A106–Gr B and A533–Gr B steels in oxygenated water to determine whether a slow strain rate applied during different portions of a tensile–loading cycle are equally effective in decreasing fatigue life. Crack growth data were obtained on fracture–mechanics specimens of SSs and Alloy 600 to investigate EAC in simulated boiling water reactor (BWR) and pressurized water reactor environments at 289°C. The data were compared with predictions from crack growth correlations developed at ANL for SSs in water and from rates in air from Section XI of the ASME Code. Microchemical changes in high– and commercial–purity Type 304 SS specimens from control–blade absorber tubes and a control–blade sheath from operating BWRs were studied by Auger electron spectroscopy and scanning electron microscopy to determine whether trace impurity elements may contribute to IASCC of these materials.

Contents

Figures

Tables

Executive Summary

Fatigue of Ferritic Piping and Pressure Vessel Steels

Plain carbon and low-alloy steels are used extensively in steam supply systems of pressurized and boiling water nuclear reactors (PWRs and BWRs) as piping and pressure vessel materials. Fatigue tests are being conducted on A106-Gr B carbon steel and A533-Gr B and A302-Gr B low-alloy steels in water and in air at 288°C to establish the effects of material and loading variables on fatigue life. The results indicate that in water with high dissolved-oxygen (DO) content, a minimum strain is required for environmentally assisted decrease in fatigue life of these steels, and a slow strain rate applied during the tensile-loading cycle decreases fatigue life more than when applied during the compressive-loading cycle. During the present reporting period, several exploratory tests were conducted on A106-Gr B and A533-Gr B steels in high-DO water in which the slow strain rate was applied during only a portion of the tensile-loading cycle to check whether each portion of the tensile cycle is equally effective in decreasing fatigue life in high-DO water. The results indicate that slow strain rates applied during any portion of the tensile-loading cycle above the threshold strain are equally damaging.

The effects of various material and loading variables, e.g., steel type, strain rate, DO, strain range, loading waveform, and surface morphology, on fatigue life of carbon and low-alloy steels in our tests are summarized in this report.

Environmentally Assisted Cracking of Alloy 600 and Wrought Stainless Steels in Simulated LWR Water

Fracture-mechanics CGR tests were conducted on compact-tension specimens of sensitized Type 304, Type 316NG, and mill-annealed Alloy 600 in oxygenated water and in deaerated water containing B, Li, and dissolved H_2 at low concentrations at 289°C. The experimental data were compared with predictions from an Argonne National Laboratory model for CGRs of stainless steels (SSs) in water and the ASME Section XI correlation for CGRs in air at the K_{max} and load-ratio values in the various tests. The data for all materials were bounded by ANL model predictions and the ASME "air line."

The effect of water chemistry on CGRs of mill-annealed Alloy 600 and sensitized Type 304 SS was explored at a load ratio of 0.95. Small amounts of chromate and sulfate (<200 ppb) and two amines (1-5 ppm) in water that contained ≈200 ppb DO produced small but measurable changes in the CGRs of the sensitized Type 304 SS specimens but had virtually no effect on the CGR of the Alloy 600 specimen. The average CGR of the Alloy 600 and sensitized Type 304 SS specimens was $\approx 2.3 \times 10^{-10}$ m·s^{-1} at an R of 0.95 and K_{max} of >30 MPa·m$^{1/2}$ under these water chemistry conditions. This rate is consistent with CGRs of sensitized Type 304 and nonsensitized Type 316NG SS specimens in oxygenated water at 289°C under similar loading conditions. The observation that different materials, e.g., Alloy 600, sensitized Type 304, nonsensitized Type 316NG, and CF-3, CF-8 and CF-8M grades of cast SSs, exhibit approximately the same CGR in oxygenated water, despite significant differences in material chemistry, microstructure, and mode of crack propagation, suggests that crack propagation is

largely controlled by the rate of cathodic reduction of DO with a concomitant anodic dissolution process at the crack tip.

Irradiation-Assisted Stress Corrosion Cracking of Type 304 SS

Slow-strain-rate tensile (SSRT) tests were performed to determine the effects of DO concentration in simulated BWR water and electrochemical potential (ECP) on susceptibility of commercial-purity (CP) Type 304 SS BWR neutron-absorber tubes to IASCC at 289°C. The results were similar to those reported by other investigators for CP-grade Type 304 SS BWR components. The threshold ECP and DO to protect the CP-grade materials against susceptibility to IASCC appear to be <-140 mV SHE and <0.01 ppm, respectively. For a fluence >1.3 x 10^{21} $n \cdot cm^{-2}$, susceptibility to IASCC seems to be determined primarily by DO or ECP.

Specimens fabricated from HP and CP heats of Type 304 SS exhibit different susceptibilities to IASCC. In comparison to the CP-grade material, susceptibility of HP-grade material was less affected by water chemistry (DO and ECP) and was significantly higher for all water chemistry and fluence conditions where cracking was observed. The HP-grade neutron-absorber tubes were characterized by more pronounced grain-boundary Cr depletion and a higher level of fluorine contamination than the CP-grade absorber tubes or control-blade sheath. The behavior of HP neutron-absorber tubes can be explained by a model based on a catalytic role of fluorine ions on corrosion at the crack tip, coupled with grain-boundary Cr depletion in the material. In the model, corrosion of fluorine-contaminated grain boundaries is accelerated because the rate of formation of a ligand complex $FeF(H_2O)_5$ is orders-of-magnitude greater than the rate to form a fluorine-free complex $Fe(H_2O)_6$. The fluorine atom is released from the labile complex $FeF(H_2O)_5$ dissolved in water when H_2O replaces the fluorine atom, thus leading to a classical catalysis by fluorine. This catalytic reaction chain is broken when the concentration of Cr ions in water is high (e.g., near Cr-rich grain boundaries), because a $CrF(H_2O)_5$ complex forms rapidly but remains inert in water. While conceptually consistent with the observed data, additional research is needed to validate the model.

Acknowledgments

The authors thank W. F. Burke, T. M. Galvin, and J. Franklin for their contributions to the experimental effort. This work is sponsored by the Office of Nuclear Regulatory Research, U.S. Nuclear Regulatory Commission, under FIN Number A2212; Program Manager: Dr. M. B. McNeil.

1 Introduction

Fatigue and environmentally assisted cracking (EAC) of piping, pressure vessels, and core components in light water reactors (LWRs) are important concerns in operating plants and for extended reactor lifetimes. The degradation processes in U.S. reactors include fatigue of austenitic stainless steel (SS) in emergency core cooling systems* and pressurizer surge line** piping in pressurized water reactors (PWRs), intergranular stress corrosion cracking (IGSCC) of austenitic SS piping in boiling water reactors (BWRs), and propagation of fatigue or stress corrosion cracks (which initiate in sensitized SS cladding) in low-alloy ferritic steels in BWR pressure vessels.*** Similar cracking has also occurred in upper-shell-to-transition-cone girth welds in PWR steam generator vessels,+ and cracks have been found in steam generator feedwater distribution piping.++ Occurrences of mechanical-vibration-and thermal-fluctuation-induced fatigue failures in LWR plants in Japan have also been documented.[1]

Another concern is failure of reactor-core internal components after accumulation of relatively high fluence. The general pattern of the observed failures indicates that, as nuclear plants age and neutron fluence increases, many apparently nonsensitized austenitic materials become susceptible to intergranular failure by a degradation process commonly known as irradiation-assisted stress corrosion cracking (IASCC). Some of these failures have been reported for components subjected to relatively low or negligible stress levels, e.g., control-blade sheaths and handles and instrument dry tubes of BWRs. Although most failed components can be replaced, some safety-significant structural components, such as the BWR top guide,+++ core plate,+++ and shroud,¶ would be very difficult or impractical to replace. Research during the past six months has focused on fatigue of ferritic steels used in piping, steam generators, and pressure vessels; EAC of wrought austenitic SSs and Alloy 600; and IASCC in high- and commercial-purity (HP and CP) Type 304 SS specimens from control-blade absorber tubes and a control-blade sheath used in operating BWRs.

2 Fatigue of Ferritic Steels (O. K. Chopra, D. J. Gavenda, and W. J. Shack)

Plain carbon and low-alloy steels are used extensively in PWR and BWR steam supply systems as piping and pressure-vessel materials. The ASME Boiler and Pressure Vessel Code Section III,[2] Subsection NB, which contains rules for the construction of Class 1 components for nuclear power plant, recognizes fatigue as a possible mode of failure in

* USNRC Information Notice No. 88-08, "Thermal Stresses in Piping Connected to Reactor Coolant Systems," June 1988; Supplement 1, June 1988; Supplement 2, August 1988; Supplement 3, April 1989.

** USNRC Information Notice No. 88-11, "Pressurizer Surge Line Thermal Stratification," December 1988.

***USNRC Information Notice No. 90-29, "Cracking of Cladding in Its Heat-Affected Zone in the Base Metal of a Reactor Vessel Head," April 1990.

+ USNRC Information Notice No. 90-04, "Cracking of the Upper Shell-to-Transition Cone Girth Welds in Steam Generators," January 1990.

++ USNRC Information Notice No. 91-19, "Steam Generator Feedwater Distribution Piping Damage," March 1991; Notice No. 93-20, "Thermal Fatigue Cracking of Feedwater Piping to Steam Generators," March 1993.

+++ USNRC Information Notice No. 95-17, "Reactor Vessel Top Guide and Core Plate Cracking," March 1995.

¶ USNRC Information Notice No. 94-42, "Cracking in the Lower Region of the Core in Boiling-Water Reactors," June 1994; Notice No. 93-79, "Core Shroud Cracking at Beltline Region Welds in Boiling-Water Reactors," September 1993.

pressure vessel steels and piping materials. Figure I–90 of Appendix I to Section III of the ASME Code specifies the fatigue design curves for the applicable structural materials. However, Section III, Subsection NB–3121 of the Code states that environmental effects on fatigue resistance of the material are not explicitly addressed in these design fatigue curves. Therefore, effects of environment on fatigue resistance of materials in all operating PWR and BWR plants whose primary coolant pressure boundary components are constructed to the specification of Section III of the Code are somewhat uncertain.

Recent fatigue strain vs. life (S–N) data from the U.S.[3–13] and Japan[14–16] illustrate potentially significant effects of LWR environments on the fatigue resistance of carbon and low–alloy steels. Specimen lives in simulated LWR environments can be nearly two orders of magnitude lower than for the corresponding tests in air. These results raise the issue of whether the fatigue design curves in Section III are appropriate for the purposes intended and whether they adequately account for effects of environment on fatigue behavior. Based on existing fatigue S–N data, researchers at ANL have developed interim fatigue design curves that take into account temperature, dissolved oxygen (DO) concentration in water, sulfur level in steel, and strain rate.[17] A statistical model has also been developed for estimating the effects of various material and loading conditions on fatigue life of carbon and low–alloy steels.[18] Results of the statistical analysis have been used to estimate the probability of initiating fatigue cracks.

The objectives of our task are to conduct fatigue tests on carbon and low–alloy steels under conditions where information is lacking in the existing S–N data base, establish the effects of material and loading variables on environmentally assisted reduction of fatigue life, and validate and update the proposed interim fatigue design curves. Fatigue tests are being conducted on A106–Gr B carbon steel and A533–Gr B and A302–Gr B low–alloy steels in water and in air at 288°C. During the present reporting period, several exploratory tests were conducted on A106–Gr B and A533–Gr B steels in which a slow strain rate is applied during only a portion of the tensile–loading cycle to check whether each portion of the tensile cycle is equally effective in decreasing fatigue life in high–DO water. The results from these tests are presented. The effects of various material and loading variables, e.g., steel type, strain rate, DO, strain range, loading waveform, and surface morphology, on fatigue life of carbon and low–alloy steels are summarized.

2.1 Experimental

Low–cycle fatigue tests are being conducted on A106–Gr B carbon steel and A533–Gr B and A302–Gr B low–alloy steels with MTS closed–loop electrohydraulics machines. The A106–Gr B material was obtained from a 508–mm–diameter, schedule 140 pipe fabricated by the Cameron Iron Works, Houston, TX. The A533–Gr B material was obtained from the lower head of the Midland reactor vessel, which was scrapped before the plant was completed. The A302–Gr B low–alloy steel had been used in a previous study of the effect of temperature and cyclic frequency on fatigue crack growth behavior in a high–temperature aqueous environment at the Bettis Atomic Power Laboratory.[19] The material showed increased CGRs in simulated PWR water at 243°C. The chemical compositions and heat treatments of the materials are given in Table 1, and the average room–temperature tensile properties are given in Table 2. The main difference between the steels is the sulfur content; i.e., 0.025% S for A302–Gr B and ≈0.015% S for A533–Gr B steel. The microstructure of the A106–Gr B carbon steel consists of pearlite,

whereas the A533–Gr B and A302–Gr B low–alloy steels contain tempered ferrite plus bainite.

Table 1. Chemical composition of ferritic steels for fatigue tests

Material	Source/ Reference[a]	Chemical Composition C	P	S	Si	Fe	Cr	Ni	Mn	Mo
					Carbon Steel					
A106–Gr B[a]	ANL	0.29	0.013	0.015	0.25	Bal	0.19	0.09	0.88	0.05
	Supplier	0.29	0.016	0.015	0.24	Bal			0.93	
A106–Gr B	Terrell	0.26	0.008	0.020	0.28	Bal	0.015	0.002	0.92	0.003
A333–Gr 6	Higuchi	0.20	0.020	0.015	0.31	Bal	–	–	0.93	–
					Low–Alloy Steel					
A533–Gr B[b]	ANL	0.22	0.010	0.012	0.19	Bal	0.18	0.51	1.30	0.48
	Supplier	0.20	0.014	0.016	0.17	Bal	0.19	0.50	1.28	0.47
A533–Gr B	JNUFAD	0.19	0.020	0.010	0.27	Bal	0.13	0.60	1.45	0.52
A302–Gr B[c]	Bettis	0.19	0.026	0.024	0.22	Bal	0.14	0.23	1.29	0.55
	Supplier	0.19	0.015	0.027	0.21	Bal	–	–	1.17	0.48

[a]508–mm–thick schedule 140 pipe fabricated by Cameron Iron Works, Heat J–7201. Actual heat treatment not known.

[b]162–mm thick hot–pressed plate from Midland reactor lower head. Austenitized at 871–899°C for 5.5 h, brine quenched and tempered at 649–663°C for 5.5 h, and brine quenched. The plate was machined to a final thickness of 127 mm. The surface was inlayed with 4.8–mm weld cladding and stress relieved at 607°C for 23.8 h.

[c]102–mm–thick thick plate. Austenitized at 899–927°C for 4 h, water quenched to 538°C, and air cooled; tempered at 649–677°C; then stress relieved at 621–649°C for 6 h (up to 6 cycles).

Table 2. Average room–temperature tensile properties of ferritic steels

Material	Reference[a]	Yield Stress (MPa)	Ultimate Stress (MPa)	Elongation (%)	Reduction in Area (%)
			Carbon Steel		
A106–Gr B	ANL	301	572	23.5	44.0
A106–Gr B	Terrell (7)	300	523	36.6	66.3
A333–Gr 6	Higuchi (11)	302	489	41.0	80.0
			Low–Alloy Steel		
A533–Gr B	ANL	431	602	27.8	66.6
A533–Gr B	JNUFAD	488	630	27.7	65.2

[a] Reference number given within parentheses.

Smooth cylindrical specimens with 9.5–mm diameter and 19–mm gage length were used for the fatigue tests. Specimen gage length was given a 1–μm surface finish in the axial direction to prevent circumferential scratches that might act as sites for crack initiation. All tests were conducted at 288°C with fully reversed axial loading (i.e., strain ratio R = –1) and a triangular or sawtooth waveform. The strain rate for the triangular wave and fast–loading half of the sawtooth wave was 0.4%/s.

A small autoclave with an annular volume of 12 mL was used for fatigue tests in water. Detailed descriptions of the test facility and procedure have been presented earlier.[11] Tests in water were performed under stroke control where the specimen strain was controlled between two locations outside the autoclave. Tests in air were performed under strain control with an axial extensometer; specimen strain between the two locations used in the water tests was also recorded. Information from the air tests was used to determine the stroke required to maintain constant strain in the specimen gage length for tests in water; the stroke is gradually increased during the test to account for cyclic hardening of the material and to maintain constant strain in the specimen gage section. The accuracy of the procedure was checked by conducting stroke-controlled tests in air and monitoring strain in the gage section of the specimen; the differences between estimated and measured strain range were ±5%.

The loading strain that is actually applied to the specimen gage section (solid line) during a stroke-controlled tests with a sawtooth waveform (dashed line) is shown in Fig. 1. However, during the cycle the fraction of applied displacement that goes to the specimen gage section is not constant but varies with the loading strain. Consequently, the loading rate also varies during the fatigue cycle; it is lower than the applied strain rate at strain levels below the elastic limit and higher at larger strains.

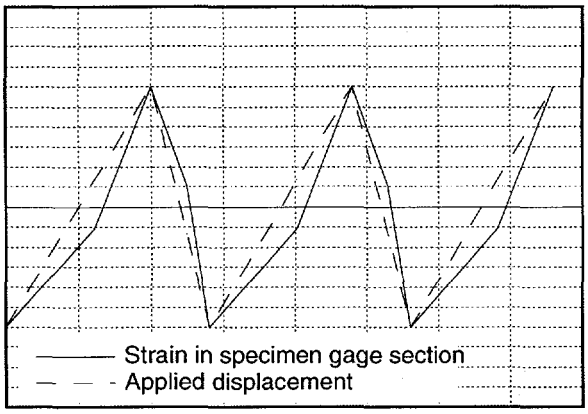

Figure 1.
Waveforms for applied displacement (dashed line) and strain in specimen gage section (solid line) during stroke-controlled test

2.2 Air Environment

The fatigue results on A106-Gr B, A533-Gr B, and A302-Gr B steels are summarized in Tables 3, 4, and 5, respectively. Fatigue S-N curves for carbon and low-alloy steels in air are shown in Fig. 2. Fatigue life is defined as the number of cycles N_{25} for tensile stress to drop 25% from its peak value; this corresponds to a ≈3-mm deep crack in the test specimen. Results from other investigations[7,14] on similar steels with comparable composition and the ASME Section III mean-data curve at room temperature are also included in the figures.

The results indicate that the fatigue life of low-alloy steels is greater than that of the carbon steel. Strain rate has little or no effect on fatigue life of A106-Gr B and A533-Gr B steels in air. The data for A106-Gr B steel are in good agreement with results obtained by Terrell[7] on A106-Gr B steel, but are lower by a factor of ≈5 than those obtained by Higuchi and Iida[14] on A333-Gr 6 steel. Also, the data for A106-Gr B steel are

Table 3. Fatigue test results for A106–Gr B carbon steel

Test Number	Environment[a]	Dissolved Oxygen (ppb)	pH at RT	Conductivity (mS/cm)	Tensile Rate (%/s)	Comp. Rate (%/s)	Stress Range (MPa)	Strain Range (%)	Life N_{25} (Cycles)
1498	Air	–	–	–	0.4	0.4	1001.4	1.004	1,048
1546	Air	–	–	–	0.4	0.4	975.7	0.916	1,365
1553	Air	–	–	–	0.4	0.4	921.1	0.757	3,253
1554	Air	–	–	–	0.4	0.4	896.8	0.730	3,753
1674[b]	Air	–	–	–	0.4	0.4	1003.6	0.764	6,275
1686[b]	Air	–	–	–	0.4	0.4	1017.2	0.804	2,592
1731	Air	–	–	–	0.4	0.004	1005.5	0.758	3,485
1615	Air	–	–	–	0.04	0.4	959.8	0.755	3,873
1609	Air	–	–	–	0.004	0.4	1026.0	0.756	3,721
1612	Air	–	–	–	0.004	0.4	1008.2	0.779	3,424
1673	Air	–	–	–	0.004	0.4	1003.6	0.759	6,275
1548	Air	–	–	–	0.4	0.4	831.9	0.545	10,632
1543	Air	–	–	–	0.4	0.4	818.2	0.502	14,525
1619	Air	–	–	–	0.4	0.4	741.7	0.401	37,142
1636[c]	Air	–	–	–	0.4	0.4	749.6	0.402	34,829
1621	Air	–	–	–	0.01	0.4	787.1	0.403	38,128
1638[d]	Air	–	–	–	0.4	0.4	800.0	0.436	26,728
1550	Air	–	–	–	0.4	0.4	681.7	0.353	66,768
1552	Air	–	–	–	0.4	0.4	680.6	0.352	93,322
1555	Air	–	–	–	0.4	0.4	676.3	0.343	98,456
1644	Air	–	–	–	0.004	0.4	702.0	0.364	>94,657
1738[e]	DI	1	6.5	0.09	0.004	0.4	976.2	0.777	1,350
1744[e]	DI	<1	6.5	0.08	0.4	0.4	760.5	0.414	19,860
1547	PWR	8	6.7	23.26	0.4	0.4	1010.9	0.987	692
1564	PWR	12	6.6	21.74	0.4	0.4	942.0	0.769	1,525
1676	PWR	2	6.5	20.83	0.4	0.4	926.7	0.741	2,230
1679	PWR	3	6.5	20.41	0.004	0.4	1005.8	0.763	2,141
1681	PWR	1	6.5	20.00	0.0004	0.4	1015.7	0.764	2,672
1549	PWR	8	6.7	25.64	0.4	0.4	827.0	0.533	9,396
1560	PWR	12	6.6	23.73	0.4	0.4	701.3	0.363	35,190
1556	PWR	8	6.6	22.73	0.4	0.4	710.9	0.360	38,632
1632	Hi DO	800	5.8	0.11	0.4	0.4	913.3	0.740	2,077
1705	Hi DO	650	5.9	0.15	0.4	0.4	947.9	0.767	1,756
1680[b]	Hi DO	700	6.0	0.08	0.4	0.4	999.6	0.818	1,007
1690[b]	Hi DO	700	6.0	0.08	0.4	0.4	1002.2	0.824	1,092
1687[f]	Hi DO	700	6.0	0.10	0.4	0.4	1020.0	0.809	840
1693	Hi DO	650	6.0	0.10	0.04	0.4	920.0	0.737	1,125
1614	Hi DO	400	5.9	0.11	0.004	0.4	930.4	0.786	303
1682	Hi DO	700	6.0	0.09	0.004	0.4	921.1	0.746	469
1623	Hi DO	800	5.9	0.08	0.004	0.004	943.8	0.792	338
1616	Hi DO	800	5.8	0.08	0.0004	0.4	912.8	0.799	153
1620	Hi DO	900	5.9	0.11	0.00004	0.004	943.1	0.794	161
1706	Hi DO	600	5.9	0.07	0.4	0.4	825.2	0.528	7,858
1634	Hi DO	800	5.8	0.16	0.4	0.4	733.2	0.400	19,318
1637[d]	Hi DO	900	5.9	0.11	0.4	0.4	788.3	0.470	16,622
1624	Hi DO	800	5.9	0.10	0.004	0.4	775.7	0.456	2,276
1639	Hi DO	800	5.9	0.09	0.004	0.4	751.6	0.418	2,951
1643	Hi DO	800	6.0	0.11	0.004	0.4	698.5	0.363	>65,000

[a] DI = Deionized water and PWR = simulated PWR water containing 2 ppm lithium and 1000 ppm boron.
[b] Tested with 5–min hold period at peak tensile strain.
[c] Specimen preoxidized at 288°C in water with 600 ppb DO for 100 h.
[d] Prior to the test, specimen was fatigued for 570 cycles in 800 ppb DO water, 0.46% strain range, with sawtooth waveform.
[e] Prior to being tested in low–DO water, specimen preoxidized at 288°C in water with 600 ppb DO for 30 h.
[f] Tested with 30–min hold period at peak tensile strain.

Table 4. Fatigue test results for A533–Gr B low–alloy steel

Test Number	Environ–ment[a]	Dissolved Oxygen (ppb)	pH at RT	Conducti –vity (mS/cm)	Tensile Rate (%/s)	Comp. Rate (%/s)	Stress Range (MPa)	Strain Range (%)	Life N_{25} (Cycles)
1508	Air	–	–	–	0.4	0.4	910.9	1.002	3,305
1524	Air	–	–	–	0.4	0.4	892.3	0.950	3,714
1523	Air	–	–	–	0.4	0.4	898.6	0.917	2,206
1521	Air	–	–	–	0.4	0.4	889.4	0.910	3,219
1522	Air	–	–	–	0.4	0.4	905.4	0.899	3,398
1515	Air	–	–	–	0.4	0.4	866.1	0.752	6,792
1717	Air	–	–	–	0.4	0.004	884.6	0.758	6,217
1625	Air	–	–	–	0.004	0.4	887.7	0.757	4,592
1629[b]	Air	–	–	–	0.4	0.4	782.9	0.503	31,243
1590	Air	–	–	–	0.4	0.004	821.1	0.503	24,471
1576	Air	–	–	–	0.004	0.4	805.8	0.503	28,129
1505	Air	–	–	–	0.4	0.4	767.6	0.501	31,200
1525	Air	–	–	–	0.4	0.4	743.6	0.452	65,758
1640	Air	–	–	–	0.4	0.4	710.9	0.402	65,880
1538	Air	–	–	–	0.4	0.4	708.0	0.387	>1,000,000
1517	Air	–	–	–	0.4	0.4	692.5	0.353	2,053,295
1659	Air	–	–	–	0.004	0.4	656.2	0.343	>114,294
1526	DI	–	–	–	0.4	0.4	876.4	0.873	3,332
1527	DI	–	6.0	–	0.4	0.4	752.8	0.493	10,292
1528	DI	5	5.8	–	0.4	0.4	744.1	0.488	25,815
1743[c]	DI	<1	6.5	0.08	0.4	0.4	712.6	0.386	84,700
1530	PWR	3	6.9	41.67	0.4	0.4	885.5	0.894	1,355
1545	PWR	8	6.9	22.73	0.4	0.4	889.7	0.886	3,273
1533	PWR	4	6.9	45.45	0.004	0.4	916.0	0.774	3,416
1529	PWR	3	6.9	45.45	0.4	0.4	743.4	0.484	31,676
1605	PWR	9	6.5	23.81	0.4	0.004	785.2	0.460	>57,443
1588	PWR	6	6.5	23.26	0.004	0.4	828.7	0.514	15,321
1539	PWR	6	6.8	38.46	0.4	0.4	690.9	0.373	136,570
1542	PWR	6	6.6	27.03	0.4	0.4	631.8	0.354	>1,154,892
1645	Hi DO	800	6.1	0.07	0.4	0.4	831.1	0.721	2,736
1626	Hi DO	900	5.9	0.13	0.004	0.4	910.1	0.788	247
1715	Hi DO	600	5.9	0.08	0.004	0.4	904.1	0.813	381
1711	Hi DO	630	5.8	0.31	0.4	0.4	772.1	0.542	5,850
1707	Hi DO	650	5.9	0.08	0.4	0.004	803.0	0.488	3,942
1709	Hi DO	650	5.9	0.11	0.4	0.004	805.1	0.501	3,510
1627	Hi DO	800	5.9	0.10	0.004	0.4	826.8	0.534	769
1641	Hi DO	800	5.9	0.09	0.4	0.4	693.0	0.385	17,367
1665	Hi DO	800	6.1	0.08	0.004	0.4	717.0	0.376	3,455
1666	Hi DO	750	6.1	0.09	0.0004	0.4	729.6	0.376	>7,380
1647	Hi DO	800	6.1	0.09	0.4	0.4	688.0	0.380	26,165
1660	Hi DO	750	6.1	0.11	0.004	0.4	689.6	0.360	>83,024
1649	Hi DO	700	6.3	0.08	0.4	0.4	673.4	0.352	28,710
1652	Hi DO	700	6.1	0.09	0.4	0.4	638.1	0.328	56,923
1655	Hi DO	750	6.1	0.10	0.4	0.4	567.6	0.289	>1,673,954

[a] DI = Deionized water and PWR = simulated PWR water containing 2 ppm lithium and 1000 ppm boron.
[b] Specimen preoxidized in water with 600 ppb DO for 100 h at 288°C.
[c] Prior to being tested in water, specimen was preoxidized in water with 600 ppb DO for 30 h at 288°C.

below the ASME mean curve for carbon steel at high strain ranges (by a factor of 3), but are above the ASME mean curve at low strain ranges. The combined data from the present study and those obtained by Terrell[7] for A106–Gr B steel may be expressed by the relationship

$$\Delta\varepsilon_t = 0.230 + 33.66N_{25}^{-0.51}. \quad (1)$$

The results for A533–Gr B steel show good agreement with the ASME mean–data curve for low–alloy steel at room temperature and JNUFAD* data on A533–Gr B steel. The ANL data for A533–Gr B steel may be expressed by the relationship

$$\Delta\varepsilon_t = 0.315 + 30.99N_{25}^{-0.49}. \quad (2)$$

These equations provide reference fatigue S–N behavior in air for the ANL heats of A106–Gr B and A533–Gr B steels.

Table 5. Fatigue test results for A302–Gr B low–alloy steel

Test Number	Environment[a]	Dissolved Oxygen, ppb	pH at RT	Conductivity, μS/cm	Tensile Rate, %/s	Comp. Rate, %/s	Stress Range, MPa	Strain Range, %	Life N_{25}, Cycles
1697	Air	–	–	–	0.4	0.4	944.5	0.756	8,070
1701	Air	–	–	–	0.004	0.4	1021.4	0.757	4,936
1712	Air	–	–	–	0.0004[b]	0.4	1041.9	0.759	5,350
1702	PWR	3.0	6.5	20.00	0.4	0.4	921.2	0.735	6,212
1704	PWR	3.0	6.5	19.23	0.004	0.4	1022.6	0.745	3,860
1716	PWR	4.5	6.5	19.23	0.0004[b]	0.4	1042.3	0.739	3,718

[a] Simulated PWR water contains 2 ppm lithium and 1000 ppm boron.
[b] Slow strain rate applied only during 1/8 cycle near peak tensile strain.

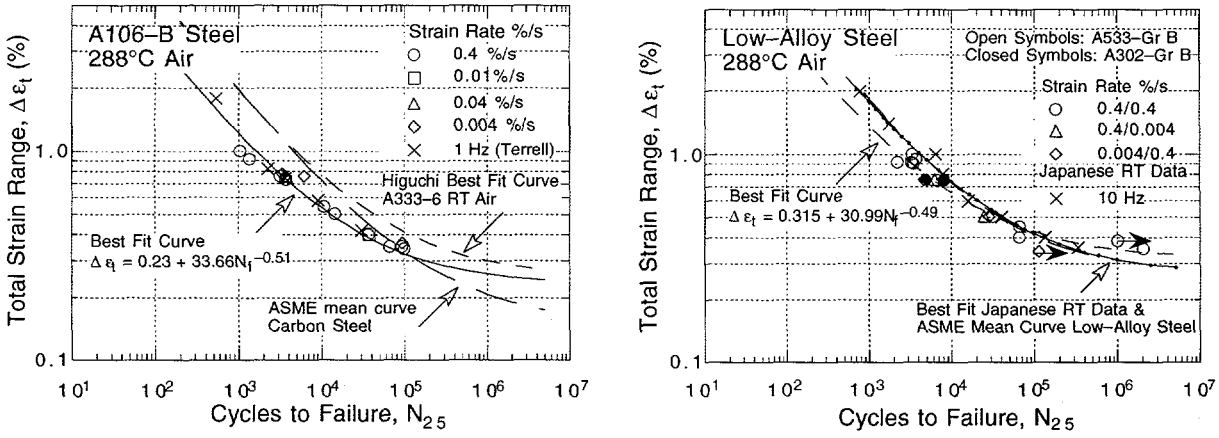

Figure 2. Total strain range vs. fatigue life data for A106–Gr B carbon steel and A533–Gr B low–alloy steel in air

The results for A302–Gr B steel are in good agreement with the data for A533–Gr B steel. However, the results indicate a possible effect of strain rate on fatigue life. For example, the fatigue life of this steel decreases by ≈40% as strain rate decreases from 0.4 to 0.004%/s, Table 5. This result is somewhat surprising because strain rate effects are not observed for the other two steels.

* Private communication from M. Higuchi, Ishikawajima–Harima Heavy Industries Co., Japan, to M. Prager of the Pressure Vessel Research Council, 1992.

2.3 Alloy Composition

The cyclic–hardening behaviors of carbon and low–alloy steels are significantly different. Plots of cyclic stress range vs. fatigue cycles for A106–Gr B and A533–Gr B steels tested in air at 288°C and total strain ranges of ≈0.75% and ≈0.35% are shown in Figs. 3 and 4, respectively. Cyclic strain–hardening of the steels is consistent with their microstructure. The A106–Gr B steel, with a pearlitic structure and low yield stress, exhibits rapid hardening during the initial 100 cycles of fatigue life. The extent of hardening increases with applied strain range. In contrast, the A533–Gr B and A302–Gr B low–alloy steels consist of tempered ferrite and bainitic structure, have relatively high yield stress, and show little or no initial hardening. At low strain ranges, the A533–Gr B steel shows cyclic softening during the initial 100 cycles of fatigue life (Fig. 4).

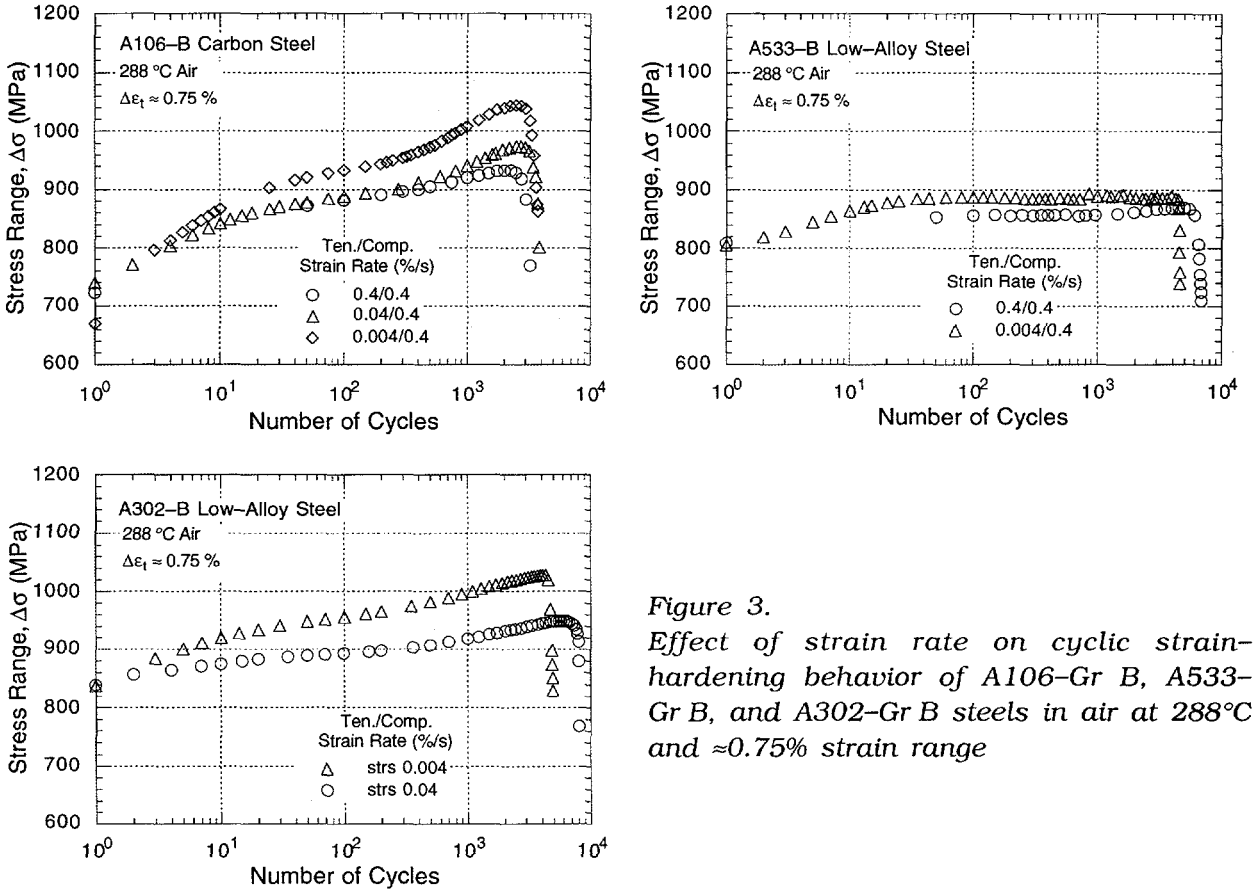

Figure 3.
Effect of strain rate on cyclic strain–hardening behavior of A106–Gr B, A533–Gr B, and A302–Gr B steels in air at 288°C and ≈0.75% strain range

Furthermore, the A106–Gr B carbon steel and A302–Gr B low–alloy steel exhibit some dynamic strain aging. Consequently, cyclic stress of these steels increases significantly with decreasing strain rate. The A533–Gr B steel exhibits little or no dynamic strain aging.

The cyclic stress vs. strain curves for A106–Gr B and A533–Gr B steels at 288°C are shown in Fig. 5; cyclic stress corresponds to the value at half life. For water environments, only the tests that exhibit a marginal (factor of 2) decrease in fatigue life, e.g., tests in simulated PWR environments or in high–DO water at high strain rates, are

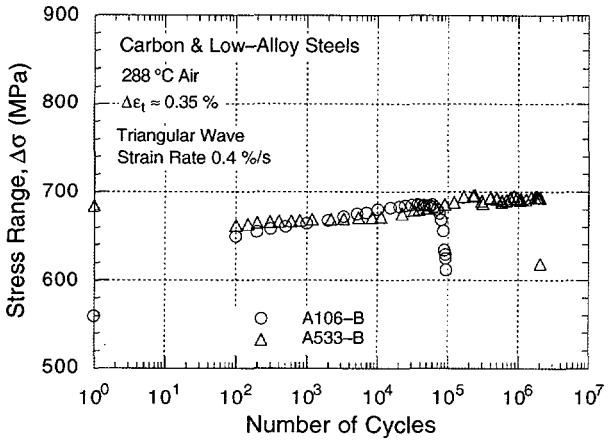

Figure 4.
Cyclic strain–hardening behavior of A106–Gr B and A533–Gr B steels at 288°C, 0.35% strain range, and 0.4 %/s strain rate in air

shown in Fig. 5. Because of decreased fatigue life of the tests in high–DO water and slow strain rates, the specimens fail before the onset of dynamic strain aging and, for these tests, cyclic stresses at half–life are significantly lower than that for the other tests (fatigue data in water are presented in next sections). The results for A106–Gr B steel show excellent agreement with the data obtained by Terrell.[7,8] The total strain range $\Delta\varepsilon_t$ (%) can be expressed in terms of the cyclic stress range (MPa) with the equation

$$\Delta\varepsilon_t = \frac{\Delta\sigma}{1965} + \left(\frac{\Delta\sigma}{C}\right)^{7.74}, \tag{3a}$$

where the constant C depends on applied strain rate $\dot{\varepsilon}$ (%/s) and is expressed as

$$C = 1080 - 50.9\,\mathrm{Log}(\dot{\varepsilon}). \tag{3b}$$

The best–fit stress vs. strain curve for A533–Gr B steel can be represented with the equation

$$\Delta\varepsilon_t = \frac{\Delta\sigma}{1965} + \left(\frac{\Delta\sigma}{D}\right)^{9.09}, \tag{4a}$$

where the constant D is expressed as

$$D = 962 - 30.3\,\mathrm{Log}(\dot{\varepsilon}). \tag{4b}$$

Crack propagation behavior is also different for the carbon and low–alloy steels. In the carbon steel, fatigue cracks propagate preferentially along the soft ferrite grains.[12] The low–alloy steel exhibits a typical straight fatigue crack propagating normal to the stress axis.

Carbon or low–alloy steel specimens develop similar surface oxide films either in air or in oxygenated water environments. In general, the specimens tested in air show slight discoloration, while the specimens tested in oxygenated water develop a gray/black corrosion scale.[11,13] X–ray diffraction analysis of the surfaces indicated that for both steels, the corrosion scale is primarily magnetite (Fe_3O_4) in simulated PWR water but may also contain some hematite (Fe_2O_3) after exposure to high–DO water. All specimens tested in water showed surface micropitting.

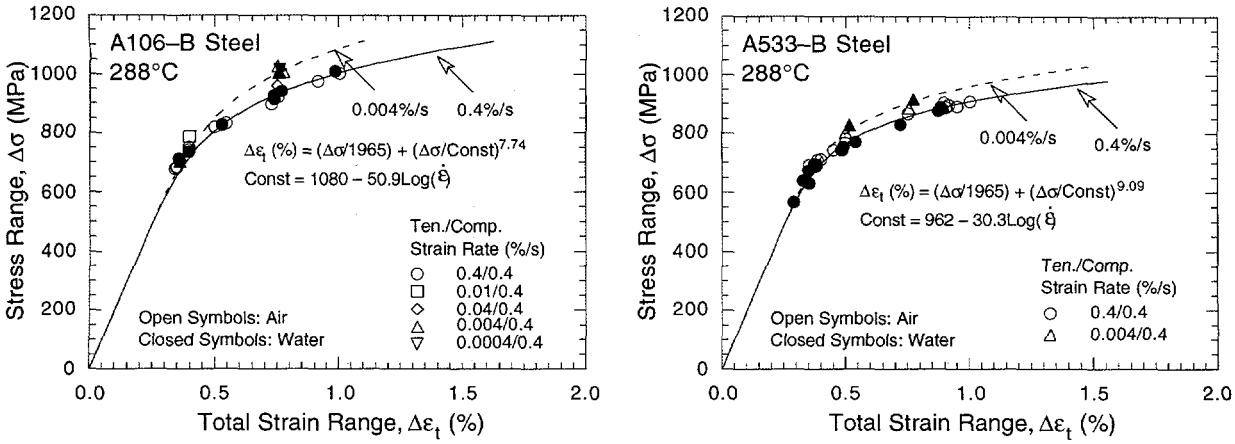

Figure 5. Cyclic stress–strain curve for A106–Gr B and A533–Gr B steels at 288°C in air and water environments

2.4 Simulated PWR Environment

Figure 6 shows the fatigue S–N plots for A106–Gr B, A533–Gr B, and A302–Gr B steels in simulated PWR water containing <10 ppb DO, 1000 ppm boron, and 2 ppm lithium. The results indicate a marginal effect of PWR water on fatigue life at high strain ranges. At strain ranges >0.5%, fatigue lives of both steels in PWR water are lower than those in air by a factor of less than 2. Furthermore, a decrease in the strain rate by three orders of magnitude does not cause an additional decrease in fatigue life of A106–Gr B and A533–Gr B steels. The results for A106–Gr B steel are consistent with the data obtained by Terrell[8] in simulated PWR water where little or no effect of strain rate or environment on fatigue life was observed. The results are also consistent with the data of Iida et al.[15] and Prater and Coffin[20,21] in which the effects of environment were minimal at DO levels of <100 ppb.

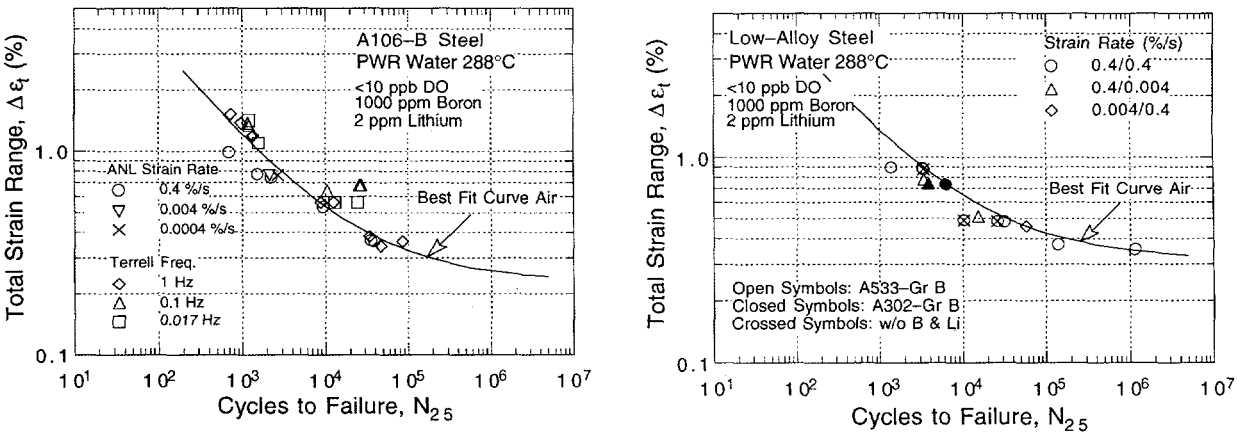

Figure 6. Strain range vs. fatigue life data for A106–Gr B and A533–Gr B steels in simulated PWR water at 288°C

The results for A302–Gr B steel also indicate only a marginal effect of PWR water on fatigue life. For a given strain rate, the fatigue life of A302–Gr B steel is lower by ≈23% in PWR water than in air. The different loading wave forms and corresponding fatigue data

for A302–Gr B steel are presented in Fig. 7. Even the 1/8–cycle slow/fast test, with a slow strain rate of 0.0004%/s, shows only a moderate decrease in fatigue life. The data suggest that even high–sulfur steels suffer only modest decreases of fatigue life in simulated PWR water. However, as was discussed earlier in Section 2.1.2, the results for A302–Gr B steel indicate a possible effect of strain rate on fatigue life. Although the steel is subject to only moderate environmental degradation of fatigue life, the fatigue life both in air and PWR water decreases by ≈40% as strain rate decreases from 0.4 to 0.004%/s. Additional fatigue specimens are being machined with the gage section orientation transverse to the rolling direction to establish possible effects of material orientation.

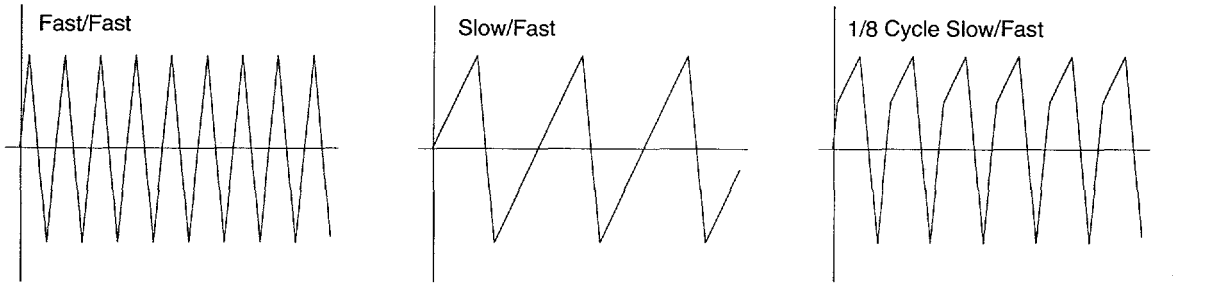

Strain rate: 0.4%/s in tension and compression		Strain rate: 0.004%/s in tension and 0.4%/s in comp.		Strain rate: 0.0004%/s during 1/8 cycle and 0.4%/s for remaining period	
Air:	8070 cycles	Air:	4936 cycles	Air:	5350 cycles
PWR:	6212 cycles	PWR:	3860 cycles	PWR:	3718 cycles

Figure 7. Fatigue life of A302–Gr B steel at 288°C in air and simulated PWR water tested with triangular or sawtooth loading wave forms at a strain range of ≈0.75%

2.5 Water with High Dissolved Oxygen

2.5.1 Strain Rate

The total strain range vs. fatigue life plots for A106–Gr B and A533–Gr B steels in water containing 0.5–0.8 ppm DO are shown in Fig. 8. The results indicate significant reductions in fatigue life and a strong dependence on strain rate. Although the microstructures and cyclic–hardening behaviors of the A106–Gr B carbon steel and A533–Gr B low–alloy steel are significantly different, there is little or no difference in environmental degradation of fatigue life of these steels. For both steels, fatigue life decreases rapidly with decreasing strain rate. Compared with tests in air, fatigue life of A106–Gr B steel in high–DO water is lower by factors of 2, 4, 10, and 18 at strain rates of 0.4, 0.04, 0.004, and 0.0004%/s, respectively. A further decrease in strain rate to 0.00004%/s does not cause additional decrease in fatigue life. The relative reduction in fatigue life is about the same whether the total strain range is 0.75 or 0.4%.

The low–alloy A533–Gr B steel shows an identical behavior. For similar test conditions, the absolute values of fatigue life for A533–Gr B low–alloy steel are comparable to those for A106–Gr B carbon steel. However, because life in air for A533–Gr B steel is greater than that for A106–Gr B steel, the relative reduction in life for the low–alloy steel is larger than that for carbon steel. This is particularly true at low strain range (0.4%), where even at the high strain rate, fatigue life is a factor of ≈10 lower than in air. These results are different than the Japanese data compiled in the JNUFAD data

base for "Fatigue Strength of Nuclear Plant Component," which indicate that environmental effects on fatigue life are greater for carbon than for low-alloy steel. However, most low-alloy steels that have been investigated in JNUFAD are low-sulfur heats, e.g., <0.007 wt.%. It is likely that differences between these two steels are caused by the sulfur content of the steels and that compositional or structural differences have only minor effects. The effects of various loading variables on fatigue life of ferritic steels in high-DO water are discussed below.

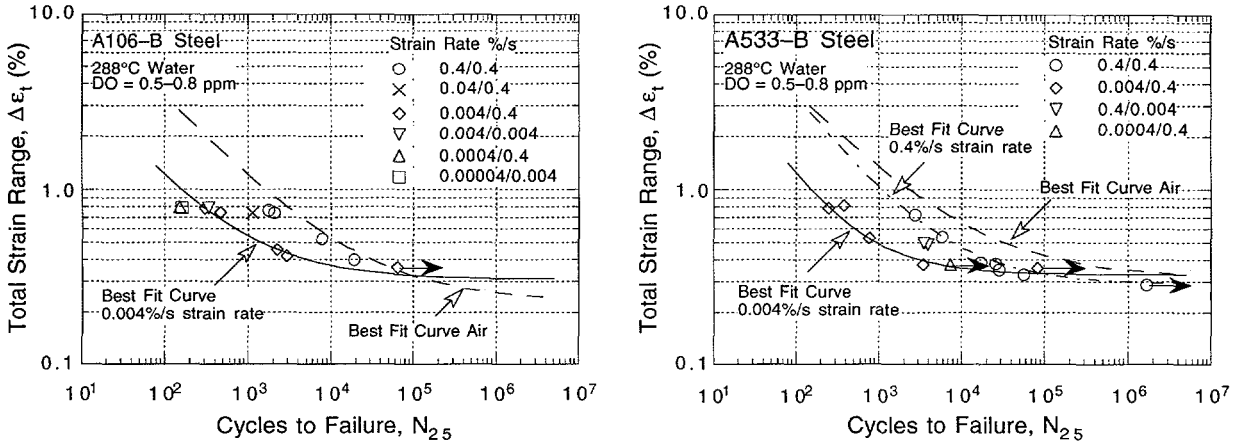

Figure 8. Total strain range vs. fatigue life data for A106-Gr B and A533-Gr B steels in high-DO water at 288°C

The relative fatigue lives of several heats of carbon and low-alloy steels are plotted as a function of strain rate in Fig. 9. Relative fatigue life is the ratio of life in water to life of that specific heat in air. The results indicate that in addition to the dependence on strain rate, environmental effects on fatigue life of carbon and low-alloy steels also depend on DO level in water and sulfur content in the steel. Fatigue life of these steels in high-DO water decreases with decreasing strain rates and increasing levels of DO and sulfur. The effect of strain rate on fatigue life appears to saturate at ≈0.001%/s strain rate.

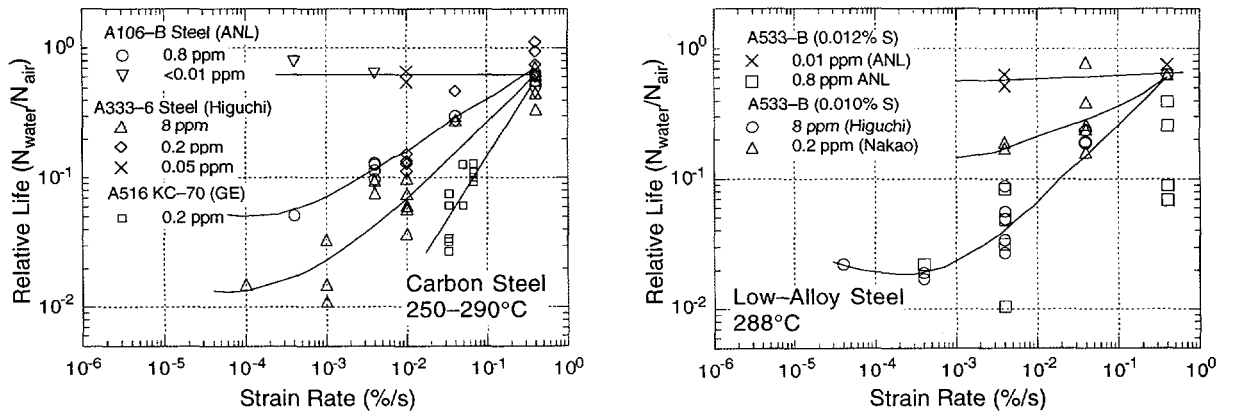

Figure 9. Relative fatigue life of several heats of carbon and low-alloy steels at different levels of dissolved oxygen and strain rate

The very-high-sulfur A516-Gr 70 carbon steel (0.033 wt.% sulfur) from the GE tests at the Dresden 1 reactor[3] shows the most severe environmental degradation. For this steel at a given strain rate, the reduction in fatigue life at 0.2 ppm DO is greater by a

factor of ≈2 than that for the A106–Gr B steel at 0.8 ppm DO and for the A333–Gr 6 steel at 0.2 ppm DO. It is unclear whether this difference is due to the extremely high sulfur level in this heat or to the loading waveform used in the Dresden tests. These tests were conducted with a trapezoidal waveform instead of the sawtooth and triangular waveforms used in the ANL and Japanese studies. The trapezoidal waveform consists of hold periods at peak tensile and compressive strains. As discussed later, a hold period at peak tensile stress also decreases fatigue life. In Fig. 9, the data points for this steel will move to the left when the contributions of the hold periods are considered.

The results presented in Fig. 8 also indicate that a slow strain rate applied during the tensile–loading cycle (slow/fast test) is primarily responsible for environmentally assisted reduction in fatigue life, and that the slow strain rate applied during the tensile– and compressive–loading cycles (slow/slow test) does not cause further decrease in fatigue life. Two fatigue tests on A106–Gr B steel at a strain range of ≈0.75%, one with a slow/fast waveform (i.e., 0.004 and 0.4%/s strain rates, respectively, during the tensile and compressive half of the loading cycle) and the other with a slow/slow waveform (i.e., 0.004%/s constant strain rate), show identical fatigue lives.

However, limited data indicate that a slow strain rate during the compressive–loading cycle (fast/slow test) may also decrease fatigue life somewhat. Two fatigue tests on A533–Gr B steel at ≈0.5% strain range and fast/slow waveform (shown as inverted triangles in Fig. 8) show a somewhat larger decrease in fatigue life than a fast/fast test, namely, a factor of 8 decrease in life for the fast/slow test compared, to a factor of 5 decrease for the fast/fast test. Additional tests are being conducted at other strain ranges and on A106–Gr B steel to determine the effects of slow strain rate during compressive–loading cycle on fatigue life.

2.5.2 Strain Range

The fatigue data in high–DO water indicate that a minimum strain is required for environmentally assisted decrease in fatigue life. This threshold value of strain range for the ANL heats of carbon and low–alloy steels appears to be at ≈0.36%; fatigue tests on A106–Gr B and A533–Gr B steels at ≈0.36% strain range, 0.6–0.8 ppm DO, and 0.004%/s tensile strain rate did not produce failure even after 65,000 and 83,000 cycles, respectively (Fig. 8). Furthermore, the fatigue S–N curves for A106–Gr B steel in air and water environments cross over at low strain ranges, i.e., fatigue life in water is longer than that in air. This apparently different fatigue S–N behavior is probably not due to the water environment. It is most likely caused by dynamic strain aging of carbon steels and is observed in Fig. 8 because of the difference in strain rate for the tests in air and water environments. The S–N curve in air is based on tests at 0.4%/s strain rate, while the curve in water represents fatigue tests at a slower strain rate of 0.004%/s. For low strain ranges, fatigue tests in water at slower strain rate show greater dynamic strain aging, higher cyclic stress, lower plastic strain range, and longer life.

2.6 Tensile Hold Period

Tests were also conducted with a 5– or 30–min hold at peak tensile strain. Loading waveforms, hysteresis loops, and fatigue lives for the tests (Fig. 10) indicate that a tensile–hold period decreases fatigue life in high–DO water but not in air. A 5–min hold period

is sufficient to reduce fatigue life; a longer hold period results in only slightly decreased life. Two 5–min–hold tests at 288°C and ≈0.8% strain range in oxygenated water with 0.7 ppm DO gave fatigue lives of 1,007 and 1,092 cycles. Fatigue life in a 30–min–hold test was 840 cycles. These tests were conducted in stroke–control mode and are somewhat different than the conventional hold–time test in strain–control mode. In the strain–control test, the total strain in the sample is held constant during the hold period. However, a portion of the elastic strain is converted to plastic strain because of stress relaxation. In a stroke–control test, there is an additional plastic strain in the sample due to relaxation of elastic strain from the load train (Fig. 10). Consequently, these are not true constant–strain–hold periods but include significant strain during the hold period; the measured plastic strains during the hold period were ≈0.028% from relaxation of the gage and 0.05–0.06% from relaxation of the load train. These conditions result in strain rates of 0.005–0.02%/s during the hold period.

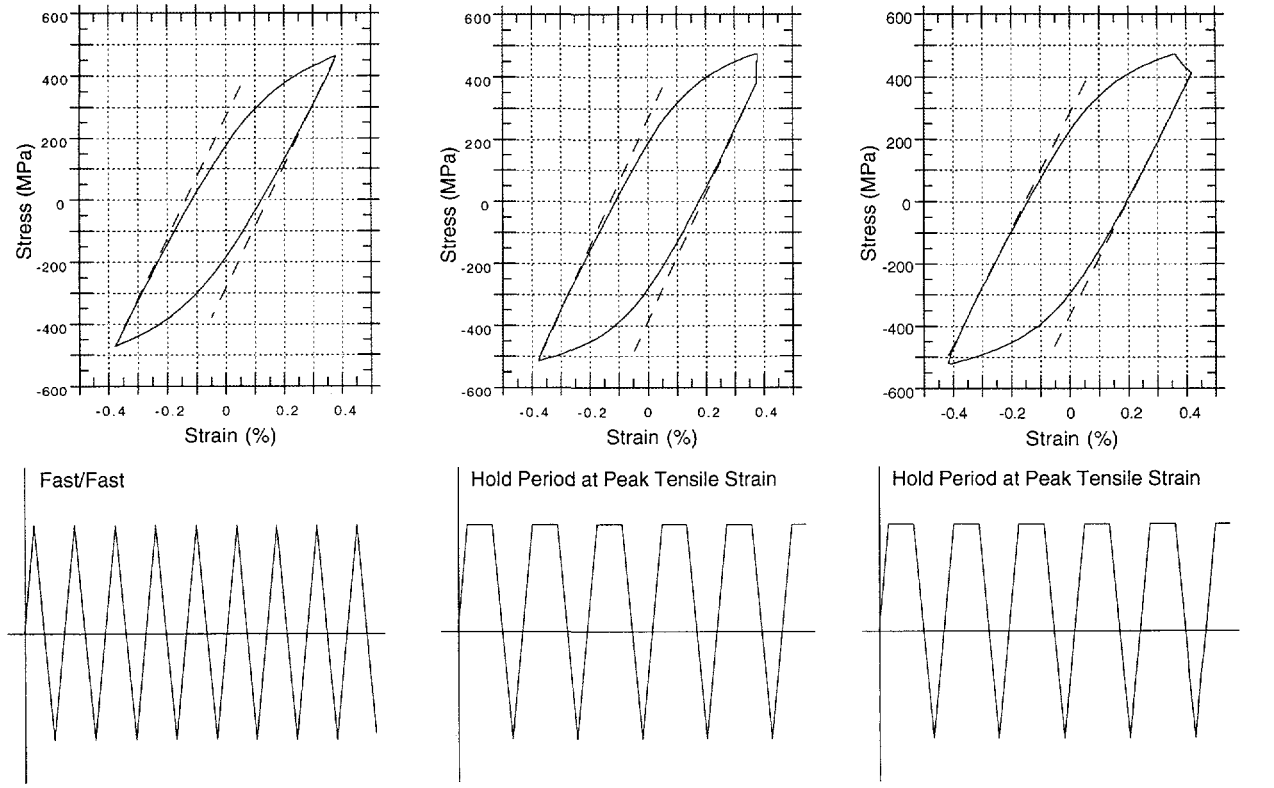

Strain or Stroke Control		Strain Control		Stroke Control (5–min hold)	
Air:	4740±1250 cycles	Air:	6,275 cycles	Air:	2592 cycles
PWR:	1965±385 cycles			High DO:	1007, 1092 cycles
High DO:	2077 cycles			Stroke Control (30–min hold)	
				High DO:	840 cycles

Figure 10. Fatigue life of A106–Gr B steel in air and water environments at 288°C, strain range of ≈0.75%, and hold periods at peak tensile strain. Hysteresis loops are for tests in air.

2.7 Surface Morphology

The fatigue crack growth behavior of ferritic steels in high–temperature oxygenated water and the effects of sulfur content and loading rate are well known.[22–29] Dissolution of MnS inclusions changes the water chemistry near the crack tip, making it more

aggressive. This results in enhanced crack growth rates because either (a) the dissolved sulfides decrease the repassivation rate, which increases the amount of metal dissolution for a given oxide rupture rate; or (b) the dissolved sulfide poisons the recombination of H atoms liberated by corrosion, which enhances H uptake by the steel at the crack tip.

The water environment may also enhance crack nucleation. For example, corrosion pits or cavities produced by dissolution of MnS inclusions can act as sites for nucleation of fatigue cracks.[30,31] A detailed metallographic examination, including measuring the cracking frequency, of the test specimens was conducted to investigate the role of surface micropitting on fatigue crack nucleation. The results have been presented elsewhere.[12] All specimens tested in water showed surface micropitting. These pits form by either corrosion of the material in oxygenated water or selective dissolution of MnS or other inclusions. However, metallographic examination of the specimens indicates that an oxygenated-water environment has no effect on the nucleation of cracks. There is no indication that fatigue cracks nucleated at any of the surface micropits. Irrespective of environment, cracks in carbon and low-alloy steels nucleate either along slip bands, carbide particles, or at the ferrite/pearlite phase boundaries. The results also show that environment has no effect on the frequency of cracks. For similar loading conditions, the number of cracks in the specimens tested in air and high-DO water are identical, although fatigue life in water is lower by a factor of ≈10.

The contributions of environment to crack nucleation were further evaluated by conducting additional exploratory tests. Figure 11 shows the fatigue life of A106-Gr B steel in air (dashed line) and in high-DO water at 0.4 and 0.004%/s strain rates (circle and diamond symbols, respectively). Fatigue tests were conducted on specimens that were preexposed at 288°C for 30–100 h in water with 0.6–0.8 ppm DO and then tested either in air or low-DO water (<10 ppb DO). At 0.4% strain range, nearly half the fatigue life may be spent in crack nucleation. Fatigue lives of the preoxidized specimens are identical to those of nonoxidized specimens; life would be expected to decrease if surface micropits facilitate crack nucleation. Similar behavior was observed for preoxidized A533-Gr B specimens.

It is possible that both the high DO and slow strain rate are needed to influence crack nucleation. This possibility was checked by first testing a specimen in high-DO water at 0.4% strain range and 0.004%/s strain rate for 570 cycles (≈25% of the life at these loading conditions) and then testing in either air or high-DO water at 0.4%/s strain rate. Fatigue life of these tests should be reduced if crack nucleation contributes in any way to environmental effects. Once again, no reduction in life is observed. These results suggest that the reduction in fatigue life in high-DO water is primarily due to environmental effects on fatigue crack propagation after nucleation of a microcrack. Environment appears to have little or no effect on crack nucleation.

2.8 Loading Waveform

Several exploratory tests were conducted on A106-Gr B and A533-Gr B steels in which a slow strain rate is applied during only a portion of the tensile-loading cycle to check whether each portion of the tensile cycle is equally effective in decreasing fatigue

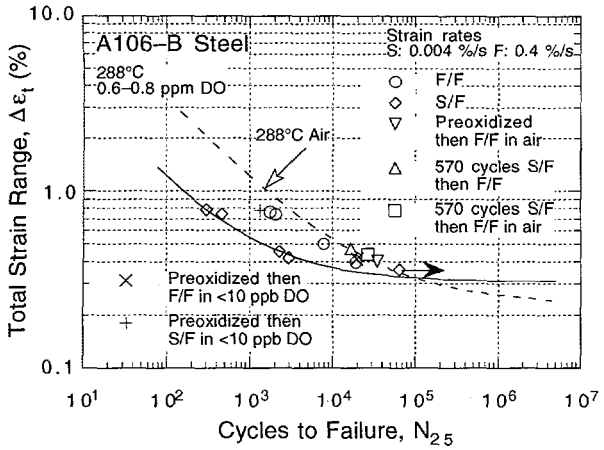

Figure 11.
Environmental effects on nucleation of fatigue crack. Preoxidized specimens were exposed at 288°C for 30–100 h in water with 0.6–0.8 ppm DO.

life in high–DO water. The results are presented in Table 6. The loading waveforms and corresponding fatigue lives for the tests on A106–Gr B steel at ≈0.75% strain range are summarized in Fig. 12. The change in fatigue life of A106–Gr B and A533–Gr B steels with fraction of loading strain at slow strain rate is shown in Fig. 13. Results are shown for slow portions applied near peak tensile strain (open symbols) or near peak compressive strain (closed symbols). In stroke–controlled tests, the fraction of loading strain that is actually applied to the specimen gage section is not constant but varies during the cycle. Consequently, for waveforms D and H, although 0.5 of the applied displacement is at a slow rate, the fractions of strain at slow rate in the specimen gage section are 0.334 and 0.666, respectively. The fraction of loading strain that is actually at slow rate for the various waveforms is given in Table 6 and Fig. 12.

At 288°C and a strain range of ≈0.75%, the average fatigue life of A106–Gr B steel in air is ≈4000 cycles. Relative to air, the fatigue lives in simulated PWR water at all strain rates or in high–DO water at high strain rates (i.e., fast/fast tests) are lower by ≈50%. If each portion of the tensile–loading cycle was equally effective in reducing fatigue life, the life should decrease linearly from A to C along the chain–dot line in Fig. 13 and a slow strain rate near peak compressive strain (waveforms D, E, or F) should be as equally damaging as a slow strain rate near peak tensile strain (waveforms H, I, or J). The results show that a slow strain rate near peak compressive strain causes no reduction in fatigue life.

As was discussed in Section 2.5.2, a minimum amount of strain is required for environmentally assisted decrease in fatigue life. This threshold strain may vary with material and loading conditions such as steel type, temperature, DO, strain ratio, mean stress, etc. For the present study, the threshold strain range for A106–Gr B carbon steel is ≈0.36%. Consequently, a slow strain rate applied during the portion of loading cycle that is below the threshold strain should have no effect on fatigue life.

This behavior is consistent with the slip–dissolution model for crack propagation;[32] the applied strain must exceed a threshold value to rupture the passive surface film in order for environmental effects to occur. (Note that this need not imply that the observed threshold strain is the actual film rupture strain. The film rupture occurs at the crack tip and is controlled by the crack tip strain. The threshold strain measured in smooth–

Table 6. Results of exploratory fatigue test in which a slow strain rate is applied only during a portion of the tensile-loading cycle

Test Number	Environment	Dissolved Oxygen (ppb)	pH at RT	Conductivity (mS/cm)	Waveform[a]	Fraction of strain at slow rate	Stress Range (MPa)	Strain Range (%)	Life N_{25} (Cycles)
A106-Gr B carbon steel									
1667	Air	–	–	–	H	0.500	999.2	0.758	5,261
1668	Air	–	–	–	I	0.250	998.5	0.758	5,139
1695	Air	–	–	–	G	0.250	993.4	0.756	5,240
1722	Air	–	–	–	E	0.250	955.8	0.758	4,087
1734	Air	–	–	–	J	0.125	970.0	0.757	4,122
1737	Air	–	–	–	F	0.125	963.7	0.757	4,105
1677	Hi DO	800	6.0	0.11	H	0.666	926.5	0.762	545
1678	Hi DO	700	5.9	0.14	I	0.347	944.4	0.780	615
1703	Hi DO	650	5.9	0.13	I	0.347	942.4	0.760	553
1698	Hi DO	600	6.1	0.08	G	0.319	909.1	0.756	1,306
1692	Hi DO	700	6.0	0.10	I[b]	0.347	936.4	0.764	261
1684	Hi DO	700	6.0	0.09	D	0.334	964.0	0.762	1,935
1728	Hi DO	700	5.9	0.07	E	0.167	969.3	0.740	1,649
1732	Hi DO	600	5.9	0.08	E	0.167	954.5	0.734	2,080
1741	Hi DO	600	6.0	0.09	J	0.170	896.8	0.785	888
1742	Hi DO	520	6.0	0.09	F	0.084	948.0	0.783	2,093
A533-Gr B low-alloy steel									
1708	Air	–	–	–	H	0.500	898.2	0.754	5,355
1710	Air	–	–	–	I	0.250	885.6	0.753	3,630
1713	Hi DO	670	5.9	0.07	H	0.666	890.8	0.761	426
1714	Hi DO	570	5.9	0.08	I	0.347	886.1	0.748	578

[a] The various waveforms are shown in Fig. 14.
[b] A slow strain rate of 0.0004%/s was used for this test.

specimen tests is a surrogate that in essence controls the crack tip strain, but no numerical equality between the two need be implied). If each portion of the loading cycle above the threshold strain is equally damaging, the decrease in fatigue life should follow line ABC when a slow rate is applied near peak tensile strain and line ADC when it is applied near peak compressive strain. The results are in agreement with this behavior, i.e., a slow strain rate applied during each portion of the loading cycle above the threshold strain is equally effective in decreasing fatigue life. Additional tests with 3/4-cycle or 7/8-cycle slow strain rates and on other heats of ferritic steels are in progress to validate these results.

3 Environmentally Assisted Cracking of Alloy 600 and Wrought SSs in Simulated LWR Water

The objective of this work is to evaluate and compare the resistance of wrought austenitic stainless steels (SSs) and nickel-base alloys to environmentally assisted cracking in simulated LWR water. Alternative materials for recirculation system piping in BWRs, e.g., Types 316NG and 347 SS, are very resistant to sensitization and thus are much less susceptible to IGSCC than Types 304 and 316 SS used in many operating reactors in the U.S. However, Type 316NG SS can undergo other modes of degradation, such as transgranular stress corrosion cracking (TGSCC) and corrosion-assisted fatigue, in simulated reactor water chemistries.

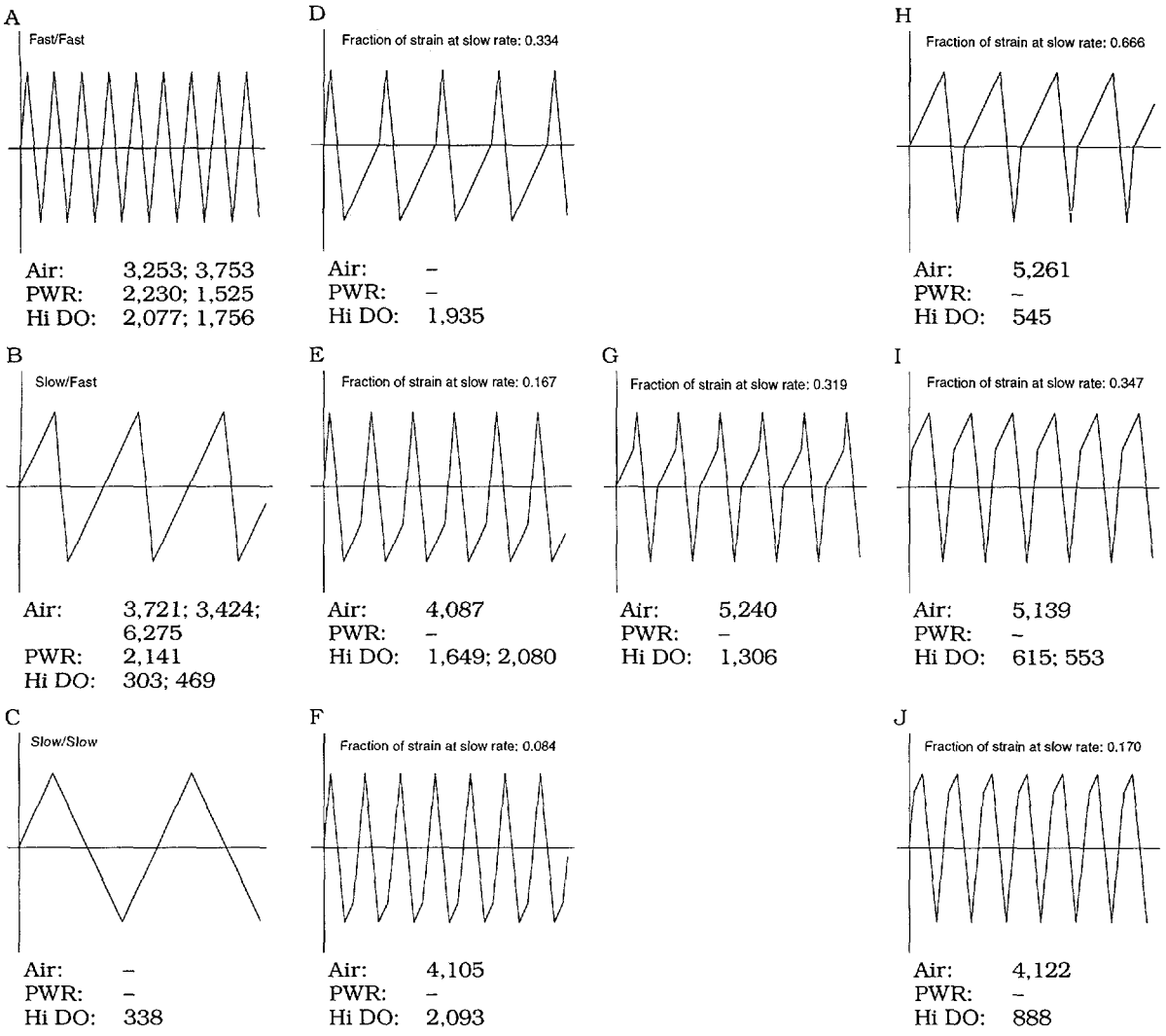

Figure 12. Fatigue life of A106–Gr B carbon steel at 288°C and 0.75% strain range in air and water environments under different loading waveforms

High–nickel alloys have experienced general corrosion (tube wall thinning) and localized intergranular attack (IGA) and SCC in LWRs. Secondary–side IGA§ and axial and circumferential SCC§§ have occurred in Alloy 600 tubes at tube support plates in many steam generators. Primary–water stress–corrosion cracking (PWSCC) of Alloy 600 steam generator tubes in PWRs at roll transitions and U–bends and in tube plugs± is a

§ USNRC Information Notice No. 91–67, "Problems with the Reliable Detection of Intergranular Attack (IGA) of Steam Generator Tubing," October 1991.

§§USNRC Information Notice No. 90–49, "Stress Corrosion Cracking in PWR Steam Generator Tubes," August 1990; Notice No. 91–43, "Recent Incidents Involving Rapid Increases in Primary–to–Secondary Leak Rate," July 1991; Notice No. 92–80, "Operation with Steam Generator Tubes Seriously Degraded," December 1992; Notice No. 94–05, "Potential Failure of Steam Generator Tubes with Kinetically Welded Sleeves," January 1994.

± USNRC Information Notice No. 89–33, "Potential Failure of Westinghouse Steam Generator Tube Mechanical Plugs," March 1989; Notice No. 89–65, "Potential for Stress Corrosion Cracking in Steam Generator Tube Plugs Supplied by Babcock and Wilcox," September 1989; Notice No. 94–87, "Unanticipated Crack in a Particular Heat of Alloy 600 Used for Westinghouse Mechanical Plugs for Steam Generator Tubes," December 1994.

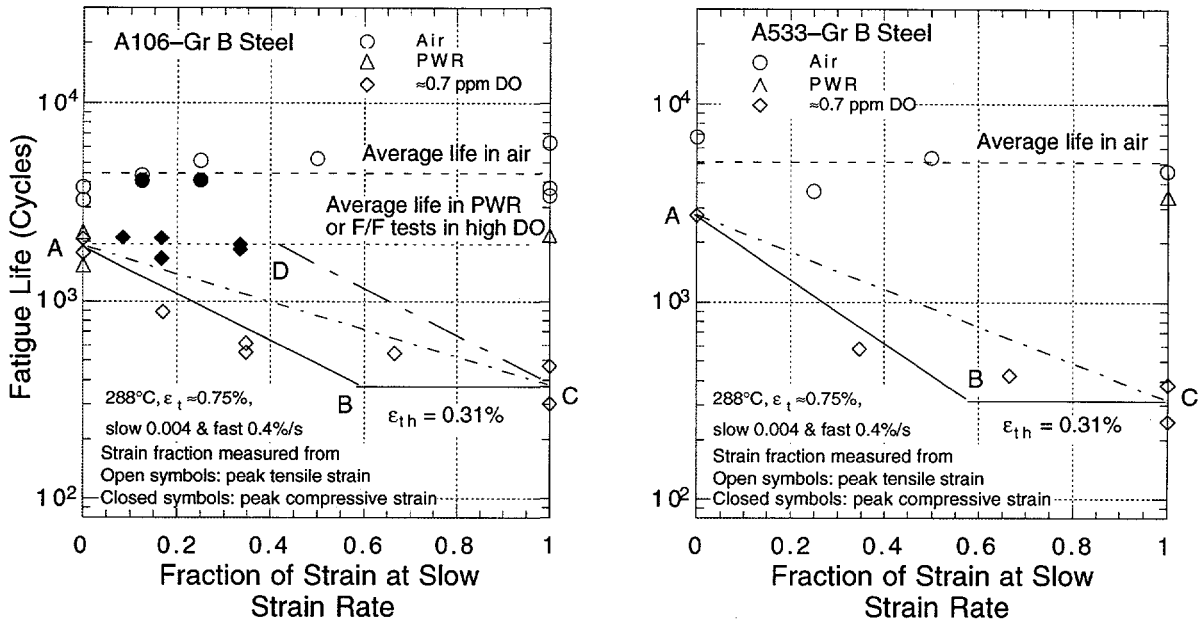

Figure 13. Fatigue life of A106–Gr B and A533–Gr B steels tested in air and water with loading waveforms where slow strain rate is applied during a fraction of tensile loading cycle

widespread problem that has been studied intensively. Cracking has also occurred in Alloy 600 and other high–nickel alloys (e.g., Inconel–82 and –182 and Alloy X750) are used for applications such as (a) instrument nozzles and heater thermal sleeves in the pressurizer† and penetrations for control–rod–drive mechanisms in the reactor vessel closure heads in the primary system of PWRs†† and (b) in dissimilar–metal weldments between SS piping and low–alloy steel nozzles, in jet pump hold–down beams,£ and in shroud–support–access–hole covers££ in BWRs. Alloy 600, in general, undergoes different thermomechanical processing for applications other than those used for steam generator tubes. Because the environmental degradation of the alloys in many cases is very sensitive to processing, further evaluation is needed even for SCC. In addition, experience strongly suggests that materials that are susceptible to SCC are also susceptible to environmental degradation of fatigue life and fatigue–crack–growth properties.

The purpose of the present work is to (a) determine the effect of load ratio and stress intensity on EAC of wrought austenitic SSs in simulated BWR and PWR water, and (b) obtain and compare CGRs of sensitized Type 304 SS, Type 316NG SS, and mill–annealed Alloy 600 in oxygenated water and in simulated PWR primary water to explore conditions where EAC occurs in all materials.

† USNRC Information Notice No. 90–10, "Primary Water Stress Corrosion Cracking (PWSCC) of Inconel 600," February 1990.

†† INPO Document SER 20–93 "Intergranular Stress Corrosion Cracking of Control Rod Drive Mechanism Penetrations," September 1993.

£ USNRC Information Notice No. 93–101, "Jet Pump Hold–Down Beam Failure," December 1993.

££ USNRC Information Notice No. 92–57, "Radial Cracking of Shroud Support Access Hole Cover Welds," August 1992.

3.1 Technical Progress (W. E. Ruther, W. K. Soppet, and T. F. Kassner)

During this reporting period, fracture-mechanics CGR tests were conducted on 1T-compact tension (CT) specimens of sensitized Type 304, Type 316NG, and mill-annealed Alloy 600 in oxygenated water and in deaerated water containing B, Li, and dissolved H_2 at low concentrations at 289°C. The composition of Types 304 and 316NG SS and Alloy 600 specimens for CGR experiments described in this report are shown in Table 7.

3.1.1 Comparison of CGRs of Sensitized Type 304 SS and Mill-Annealed Alloy 600 in Oxygenated Water

A fracture-mechanics crack-growth-rate (CGR) experiment has been conducted on Alloy 600 and two sensitized Type 304 SS specimens in simulated BWR water containing 0.2 ppm DO at conductivities in the range ≈0.08 to 8.3 $\mu S \cdot cm^{-1}$. Thirteen tests were performed on the set of three specimens during a ≈7900 h period to compare the CGR behavior of mill-annealed Alloy 600 with sensitized Type 304 SS (electrochemical potentiokinetic reactivation [EPR] values of 6 and 17 $Coulombs \cdot cm^{-2}$) in high-purity (HP) water and water containing sulfate and chromate impurities at low concentrations at 289°C. The effect of two amines (2-butanone-oxime and ethanolamine) at low concentrations (1-5 ppm) on CGRs of the materials in oxygenated water was also investigated. The test conditions and experimental results are shown in Table 8. Most of the results were obtained at a load ratio R of 0.95 and a range of K_{max} values between 28 and 41 $MPa \cdot m^{1/2}$. Load ratios of 0.6 and 0.8 were used in two of the tests. The frequency and rise time of the positive sawtooth wave form were 0.077 Hz and 12 s, respectively.

Experimental CGR data for the three specimens are plotted in Fig. 14 versus CGRs for wrought SSs in air predicted by the ASME Section XI correlation at the K_{max} and load ratio values for the specimens in the various tests. The dashed and solid lines represent Argonne National Laboratory (ANL) model predictions for crack growth in water[33] and the "air line" predicted by the ASME Code, respectively. Data for all materials are bounded by the two curves.

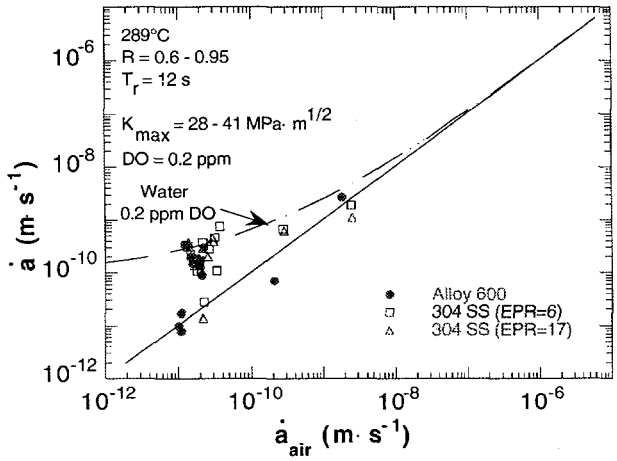

Figure 14. Corrosion fatigue data for specimens of Alloy 600 and sensitized Type 304 SS in oxygenated water at 289°C. Dashed line represents model predictions for austenitic SSs in water containing 0.2 ppm DO. Diagonal line corresponds to crack growth of SSs in air.

Table 7. Chemical composition Alloy 600 and Types 304 and 316NG SS for corrosion fatigue tests

Material	Heat	Composition (wt.%)															
	No.	Cr	Mo	Ni	Fe	Mn	Si	C	N	P	S	B	Cu	Ti	Al	Co	Nb+Ta
Alloy 600	J422	15.37	0.23	76.36	7.27	0.20	0.32	0.080	0.0145	0.016	0.004	0.0024	0.15	0.16	0.27	0.05	0.06
304 SS	10285	18.31	0.38	8.51	70.45	1.58	0.59	0.060	0.084	0.025	0.011	–	–	–	–	–	–
304 SS	30956	18.99	0.44	8.00	70.17	1.54	0.48	0.060	0.10	0.019	0.007	–	0.19	–	–	–	–
316NG	13198	16.51	2.08	10.70	68.06	1.63	0.64	0.021	0.085	0.022	0.017	–	0.21	–	–	–	0.02

Table 8. Crack growth results for Alloy 600 and sensitized[a] Type 304 SS specimens under high-R loading[b] in high-purity oxygenated water and in oxygenated water containing chromate, sulfate, 2-butanone-oxime, or ethanolamine at 289°C

Test No.	Test Time, h	Water Chemistry[c] Chromate Conc.,[d] ppb	Sulfate Conc.,[d] ppb	Other Conc., ppm	Cond. at 25°C, μS·cm^{-1}	pH at 25°C	Electrode Potential 304 SS mV(SHE)	Electrode Potential Pt mV(SHE)	Load Ratio	Material (Sensitization, EPR) Alloy 600 K_{max}[e], MPa·m$^{1/2}$	Alloy 600 Rate, 10^{-10} m·s^{-1}	304 SS (6 C·cm^{-2}) K_{max}[e], MPa·m$^{1/2}$	304 SS (6 C·cm^{-2}) Rate, 10^{-10} m·s^{-1}	304 SS (17 C·cm^{-2}) K_{max}[e], MPa·m$^{1/2}$	304 SS (17 C·cm^{-2}) Rate, 10^{-10} m·s^{-1}
1	530–1190	–	–	–	0.09	6.24	60	98	0.95	28.0	0.10	30.4	3.1	30.7	3.7
2	1190–1232	–	–	–	0.08	6.31	65	99	0.80	28.1	0.70	30.7	6.7	31.1	6.2
3	1318–1344	–	–	–	0.08	6.31	58	84	0.60	28.4	27.0	31.2	19.0	31.4	11.0
4	1390–1910	50	–	–	0.25	6.07	61	59	0.95	28.5	0.17	31.4	2.2	31.8	2.3
5	1918–2380	200	–	–	0.74	5.64	64	32	0.95	28.7	0.078	32.4	1.4	32.8	1.9
6	2385–3162	50	15	–	0.42	6.03	71	13	0.95	29.5	3.4	33.4	1.1	33.8	1.9
7	3170–3832	50	25	–	0.47	5.93	76	37	0.95	30.6	3.3	34.2	1.4	34.3	1.2
8	3865–4323	50	100	–	1.05	5.63	94	1	0.95	31.3	2.0	35.1	3.7	35.1	2.9
9	4395–5175	50	–	–	0.27	6.11	53	-23	0.95	32.0	1.5	35.5	0.28	35.3	0.14
10	5770–6475	–	–	1.0[f]	0.08	6.23	139	166	0.95	33.8	1.4	37.5	2.8	36.9	2.0
11	6490–7050	–	–	5.0[f]	0.08	6.41	163	235	0.95	34.6	1.8	39.5	4.6	38.8	4.5
12	7075–7675	–	–	–	0.08	6.27	105	160	0.95	34.8	0.90	40.1	1.1	38.8	≈0
13	7770–7910	–	–	5.0[g]	8.3	9.60	-3	-221	0.95	35.5	3.0	41.4	7.5	39.1	3.9

[a] Compact tension specimens (1TCT) of Alloy 600 (Heat No. J422) and Type 304 SS (Heat No. 10285). The Alloy 600 specimen (No. IN-1) was tested in the as-received mill-annealed condition. The Type 304 SS specimens (Heat No. 10285) received a solution-anneal heat treatment at 1050°C for 0.5 h. Specimen No. C34 was sensitized at 650°C for 2 h (EPR= 6 C·cm^{-2}) and Specimen No. C35 at 650°C for 8 h (EPR = 17 C·cm^{-2}).

[b] Frequency and rise time of the positive sawtooth waveform were 8 x 10^{-2} Hz and 12 s, respectively.

[c] Effluent dissolved-oxygen concentration was ≈200-300 ppb; feedwater oxygen concentration was higher by a factor of 3 to compensate for oxygen depletion by corrosion of the autoclave system.

[d] Chromate and sulfate were added to the feedwater as acids; average effluent chromate concentrations were ≈23 and 59 ppb for feedwater levels of 50 and 200 ppb on the basis of colorimetric analyses of grab samples.

[e] Stress intensity, K_{max}, values at the end of the time period.

[f] 2-butanone-oxime was added to the oxygenated feedwater.

[g] Ethanolamine was added to the oxygenated feedwater.

The dependence of the CGRs of Alloy 600 and sensitized Type 304 SS specimens on K_{max} at an R value of 0.95 is shown in Figs. 15 and 16, respectively, along with predictions for austenitic SSs in water from the ANL model and the ASME Code in air (dashed and solid lines, respectively). Several data points in each figure lie near the "air line" predicted by the ASME Code, i.e., there is no environmental enhancement in the rates. The results for Alloy 600 in Fig. 15 suggest a threshold K_{max} for EAC of ≈26 MPa·m$^{1/2}$ at an R of 0.95, i.e., CGRs at higher K_{max} lie significantly above the air line. The results in Fig. 16 for the sensitized Type 304 SS specimens do not exhibit a threshold K_{max} for EAC.

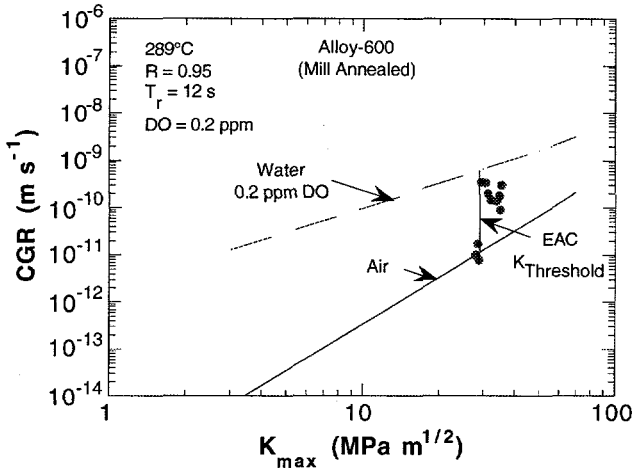

Figure 15.
Dependence of CGR of an Alloy 600 specimen on K_{max} in oxygenated water at 289°C. Dashed and solid lines represent model predictions for austenitic SSs in water containing 0.2 ppm DO and in air, respectively, at an R value of 0.95 and rise time of 12 s.

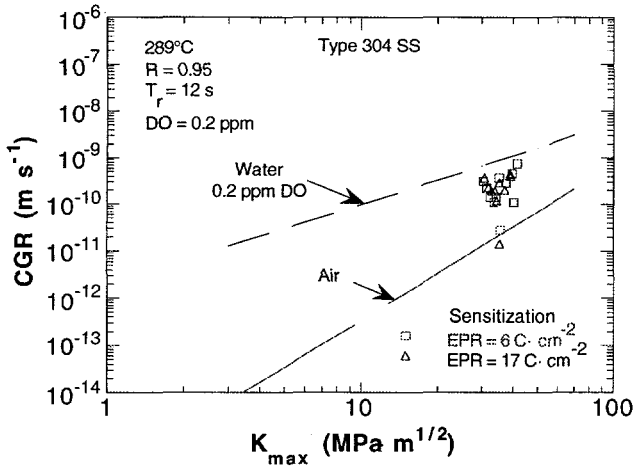

Figure 16.
Dependence of CGR of sensitized Type 304 SS specimens on K_{max} in oxygenated water at 289°C. Dashed and solid lines represent model predictions in water containing 0.2 ppm DO and in air, respectively, at an R value of 0.95 and rise time of 12 s.

To illustrate the relative effect of simulated BWR water on EAC of Alloy 600 and sensitized Type 304 SS, the CGRs of Alloy 600 are plotted versus the rates for the SS specimens under the same environmental and loading conditions in each test (Fig. 17). A data set in which the CGR of any of the three specimens was near the "air line" in Figs. 14–16 was omitted from the plot. A valid comparison of environmental effects on CGRs of the two materials can be made only when the specimens exhibit some degree of enhancement in the rates. Furthermore, CGRs of ≤3 x 10^{-11} m·s^{-1} (near the air line in Figs. 14–16) are based on small changes in crack length that are near the sensitivity of the DC potential-drop crack-length monitoring system, namely, 5 x 10^{-5} m, divided by

the test times of ≈500–800 h. This can lead to a large uncertainty in a comparison of the rates in this range. The results in Fig. 17 indicate that mill-annealed Alloy 600 and sensitized Type 304 SS have virtually the same CGR in simulated BWR water under the conditions in these tests.

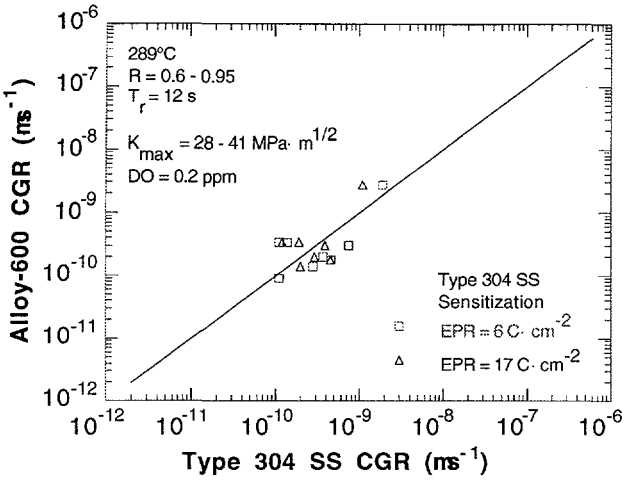

Figure 17. Comparison of CGRs of Alloy 600 and two sensitized Type 304 SS specimens under the same loading and environmental conditions at 289°C. Solid line represents identical CGRs in Alloy 600 and Type 304 SS.

The effect of water chemistry on CGRs of the materials at a load ratio of 0.95 was explored in Tests 4–13 in Table 8. Chromate additions of 50 and 200 ppb to the feedwater produced modest decreases in the CGRs of the sensitized SS specimens (Tests 1, 4, and 5). The CGRs of the Alloy 600 specimen were lower that those of the SS specimens by a factor of ≈10 and were not influenced by 50–200 ppb chromate in oxygenated water. In Tests 6–8, 15, 25, and 100 ppb of sulfate was added to water that contained 50 ppb chromate and ≈200 ppb DO. The CGRs of the sensitized Type 304 SS specimens increased by at most a factor of ≈3. The CGR Alloy 600 specimen increased from ≈8 x 10^{-12} to ≈3 x 10^{-10} m·s^{-1} when sulfate was added to the feedwater (Test 6), but the rate did not increase with sulfate concentration. When sulfate was no longer added to the oxygenated feedwater that contained 50 ppb chromate (Test 9), the CGRs of both sensitized Type 304 SS specimens decreased by a factor to 10 to ≈1–3 x 10^{-10} m·s^{-1}; the CGR of the Alloy 600 specimen remained constant at ≈1 x 10^{-10} m·s^{-1}. In the last series of experiments (Tests 10–13), chromate was no longer added to the feedwater and the effect of 1 and 5 ppm of 2-butanone-oxime or ethanolamine in water that contained ≈200 ppb DO was investigated. Under these water chemistry conditions, the CGRs of the SS specimens increased to their previous values of ≈2–4 x 10^{-10} m·s^{-1}, and once again, the Alloy 600 specimen did not respond to changes in water chemistry. These amines at a concentrations of 1–5 ppm had neither a beneficial nor deleterious effect on the CGRs of the specimens.

In summary, additions of small amounts of chromate, sulfate, and the two amines to oxygenated feedwater produced small but measurable changes in CGRs of sensitized SS specimens but had virtually no effect on CGRs of the mill-annealed Alloy 600 specimen. If the effects of these species in oxygenated water are neglected, the average CGRs of the Alloy 600 and sensitized Type 304 SS (EPR = 6 and 17 C·cm2) specimens are 2.16 x 10^{-10}, 2.65 x 10^{-10}, and 2.22 x 10^{-10} m·s^{-1}, respectively, at an R of 0.95 and K_{max} of >30 MPa·$m^{1/2}$. These values, i.e., ≈2 x 10^{-10} m·s^{-1}, are consistent with numerous

determinations of EAC of sensitized Type 304 and nonsensitized Type 316NG SS specimens in oxygenated water at 289°C under similar loading conditions.[34] We have observed that different materials, e.g., Alloy 600, sensitized Type 304, nonsensitized Type 316NG, and CF-3, CF-8 and CF-8M grades of cast SSs,[35] exhibit the same CGR in oxygenated water despite significant differences in material chemistry and microstructure. Because these materials exhibit different modes of crack propagation albeit at the same rate, i.e., sensitized SSs and low-carbon nuclear grade SSs exhibit intergranular and transgranular modes, whereas cracks in cast grades of austenitic SSs propagate along austenite/ferrite grain boundaries, suggests that the rate of crack propagation is controlled by the rate of cathodic reduction of DO, with a concomitant anodic dissolution process at the crack tip.

3.1.2 Comparison of CGRs of Sensitized Type 304 SS, Type 316NG SS, and Mill-Annealed Alloy 600 in Oxygenated Water and in Simulated PWR Water

Specimens of Alloy 600, Type 316NG, and sensitized Type 304 SS (EPR = 20 $C \cdot cm^{-2}$) were assembled in another autoclave system to determine CGRs at high load ratios in simulated PWR water where an environmental contribution to cracking may be significant at 289°C. Initial tests were conducted in water containing 450 ppm B and 2.25 ppm Li (added to the feedwater as H_3BO_3 and LiOH), 4.1 $cm^3 \cdot kg^{-1}$ H_2, ≈1 ppb DO, and 750 ppb hydrazine. The room-temperature pH and conductivity were ≈7.2 and 42 $\mu S \cdot cm^{-1}$, respectively. Hydrazine was added to the feedwater to scavenge residual DO to a very low level; however, it raised conductivity from ≈25 to 42 $\mu S \cdot cm^{-1}$. Effluent-dissolved O_2 and H_2 concentrations were determined by Orbisphere oxygen and hydrogen meters. The Alloy 600 specimen was in the as-received mill-annealed condition and the Type 316NG and 304 SS specimens were solution-annealed at 1050°C for 0.5 h and given sensitization heat treatments at 650°C for 24 h (EPR = ≈0 $C \cdot cm^{-2}$) and at 700°C for 12 h (EPR = 20 $C \cdot cm^{-2}$), respectively. Crack growth rates were determined by the DC potential-drop method.

The usual technique to initiate a fatigue crack in the specimens at 289°C in the test environment at a K_{max} of 20 $MPa \cdot m^{1/2}$, a load ratio of 0.2, and a frequency of 10 Hz was successful for the SS specimens, but a fatigue crack did not initiate in the Alloy 600 specimen. In an attempt to initiate a crack in the latter specimen, the K_{max} and load ratio were increased to 30 $MPa \cdot m^{1/2}$ and 0.8, respectively. Under these conditions, the CGRs of the Type 316NG and 304 SS specimens were ≈3.0 x 10^{-10} and 23.0 x 10^{-10} $m \cdot s^{-1}$, respectively, but once again no crack growth had occurred in the Alloy 600 specimen (Test 1 in Table 9). Because of the high CGRs of the SS specimens, the load ratio was increased from 0.8 to 0.9 in the next test. Under this condition, crack growth occurred in the Alloy 600 specimen, but the DC potential-drop measurements indicated small negative CGRs for both SS specimens. Although we could not identify the origin of the problem, we have never been encountered this behavior in tests in simulated BWR water. Consequently, the water chemistry was changed from simulated primary PWR water to HP water that contained ≈6 ppm DO for series of tests at load ratios between 0.2 and 1.0 (Tests 3-8 in Table 9). In this environment, CGRs were determined for the three specimens. Then, another attempt was made to determine CGRs in simulated PWR water

Table 9. Crack growth results for Alloy 600, Type 316NG, and sensitized[a] Type 304 SS specimens in simulated PWR and high-purity oxygenated water at 289°C

Test No.	Test Time, h	Water Chemistry: B[b] Conc., ppm	Li[b] Conc., ppm	H_2[c] Conc., cc·kg^{-1}	O_2[c] Conc., ppm	Cond. at 25°C, μS·c m^{-1}	pH at 25°C	Electrode Potential: 304 SS mV(SHE)	Alloy 600 mV(SHE)	Load Ratio[d]	Material (Sensitization, EPR): Alloy 600 K_{max}[e], MPa·m$^{1/2}$	Alloy 600 Rate, 10^{-10} m·s^{-1}	316NG SS K_{max}[e], MPa·m$^{1/2}$	316NG SS Rate, 10^{-10} m·s^{-1}	304 SS (20 C·cm^{-2}) K_{max}[e], MPa·m$^{1/2}$	304 SS (20 C·cm^{-2}) Rate, 10^{-10} m·s^{-1}
1	74–113	450	2.25	4.1	0.001[f]	41.7	7.23	-666	-668	0.8	29.4	-[g]	30.3	2.97	31.0	22.9
2	118–230	450	2.25	4.1	0.001[f]	41.7	7.27	-731	-693	0.9	29.4	0.96	30.3	-[g]	31.0	-[g]
3	304–327	0	0	0	6.0	0.07	6.09	122	45	0.8	31.7	2.67	30.4	15.8	32.3	43.5
4	335–397	0	0	0	6.0	0.07	6.09	122	45	1.0	5.8	-[g]	5.6	0.27	6.0	2.95
5	409–422	0	0	0	5.8	0.07	6.09	128	48	1.0	15.8	0.48	15.5	0.72	16.5	2.13
6	471–481	0	0	0	5.8	0.07	6.09	142	53	0.5	31.7	2.37	32.0	189.0	33.6	95.0
7	495–501	0	0	0	5.8	0.07	6.09	142	53	0.2	33.1	98.0	39.2	399.0	40.5	361.0
8	504–545	0	0	0	5.2	0.07	6.09	142	55	0.8	32.7	5.72	38.9	13.4	40.3	22.8
9	640–688	450	2.25	4.0	0.001[f]	38.5	7.55	-748	-766	0.8	30.7	16.0	39.7	31.0	-	-[h]
10	718–788	450	2.25	45.3	0.001[f]	41.6	7.31	-783	-315	0.8	30.7	0.36	42.5	45.0	-	-[h]

[a] Compact tension specimens (1TCT) of Alloy 600 (Heat No. J422), Type 316NG (Heat No. 13198), and Type 304 SS (Heat No. 30956). The Alloy 600 specimen (No. IN-2) was tested in the as-received mill-annealed condition. Type 316NG and 304 SS specimens (Nos. 198-2 and 37, respectively) received a solution-anneal heat treatment at 1050°C for 0.5 h and were given sensitization heat treatments at 650°C for 24h (EPR= ~0 C·cm^{-2}, No. 198-2) and at 700°C for 12h (EPR = 20 C·cm^{-2}, No. 37).

[b] Boron and lithium were added to the feedwater as H_3BO_3 and LiOH.

[c] Effluent dissolved H_2 and O_2 concentrations were determined with an Orbisphere hydrogen and oxygen meters.

[d] Frequency and rise time of the positive sawtooth waveform were 8 x 10^{-2} Hz and 12 s, respectively, at load ratio values of <1.0.

[e] Stress intensity, K_{max}, values at the end of the time period.

[f] Effluent dissolved-oxygen concentration was ≈1 ppb; ≈750 ppb hydrazine was added to deoxygenated feedwater to scavenge residual dissolved oxygen.

[g] Crack length measurements by the dc potential-drop method indicated small negative crack growth rates.

[h] The dc potential-drop method indicated eratic large negative crack growth rates.

by the DC potential-drop method in Tests 9 and 10. Once again, data for one of the SS specimens became erratic but results for the other and the Alloy 600 specimen exhibited normal variability. In the last test (No. 10), hydrogen concentration was increased from ≈4 to 45 $cm^3 \cdot kg^{-1}$ to determine its effect on the CGR of the Alloy 600 specimen at a load ratio of 0.8 and a K_{max} of ≈31 $MPa \cdot m^{1/2}$. This hydrogen concentration produced a decrease in the CGR of the Alloy 600 specimen by a factor of ≈40 and a relatively small increase (45%) in the CGR of the Type 316NG SS specimen. The experiment was terminated and the system is being reconfigured to utilize the crack-opening-displacement (COD) compliance technique for crack length measurements on specimens of Alloy 600 and 690 in simulated PWR water with a range of hydrogen concentrations.

Experimental CGR data for the Alloy 600 and Type 304 and 316NG SS specimens in HP water containing ≈6 ppm DO are plotted in Fig. 18 versus CGRs for wrought SSs in air predicted by the ASME Section XI correlation at the K_{max} and load ratio values for the specimens in the various tests. The dashed and solid lines represent ANL model predictions for crack growth in water[33] and the "air line" predicted by the ASME Code, respectively. With exception of one data point for Alloy 600, the results are bounded by the two curves.

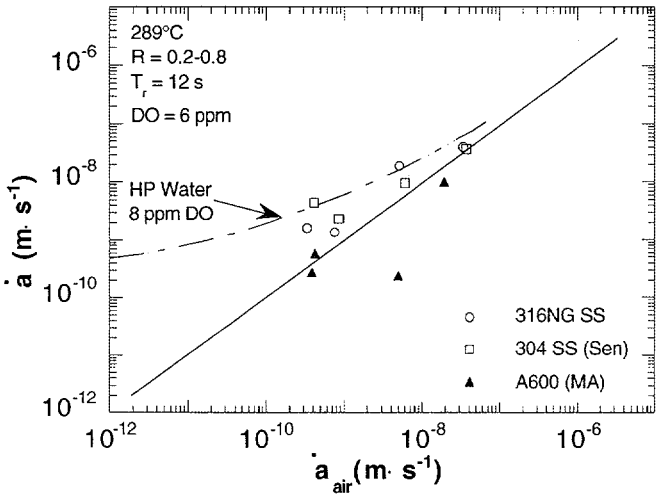

Figure 18. Corrosion fatigue data for specimens of Alloy 600, Type 316NG and sensitized Type 304 SS in oxygenated water at 289°C. Dashed line represents model predictions for austenitic SSs in water containing 8 ppm DO. Diagonal line corresponds to crack growth of SSs in air.

The dependence of CGRs of the austenitic SS specimens on load ratio at K_{max} values of 6-43 $MPa \cdot m^{1/2}$ is shown in Fig. 19 along with the dependence predicted by the ANL model for austenitic SSs in water that contains 8 ppm DO at a K_{max} of 35 $MPa \cdot m^{1/2}$. The model prediction provides a good upper-bound estimate of the CGRs at all load ratios. The data at constant load shown in the figure are also consistent with extrapolation of the corrosion-fatigue curve to R = 1. These data were obtained at low values of stress intensity (≈6 and 16 $MPa \cdot m^{1/2}$ in Table 9); therefore, model predictions at lower K_{max} values would be more consistent with the data.

Figure 20 shows experimental CGR data for the Alloy 600 and Type 304 and 316NG SS specimens in simulated PWR primary system water containing ≈1 ppb DO versus CGRs for wrought SSs in air predicted by the ASME Section XI correlation at the K_{max} and load ratio values for the specimens in the various tests. The dashed lines represents the ANL model prediction for crack growth in water that contains ≈1 ppb DO and no

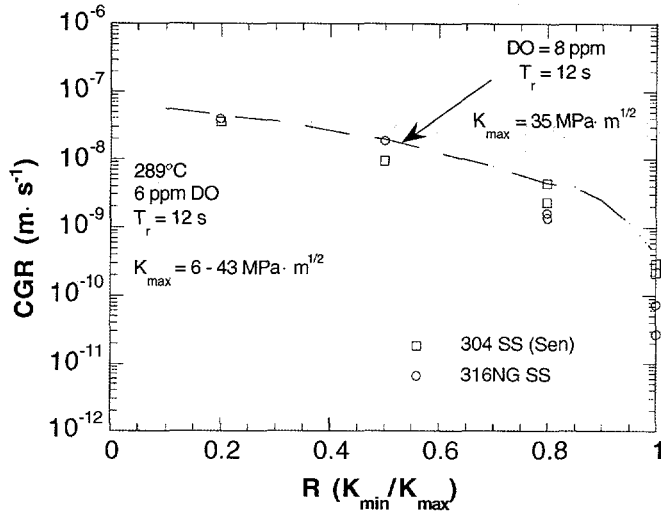

Figure 19.
Dependence of CGR of Type 316NG and sensitized Type 304 SS on load ratio in HP oxygenated water at 289°C. Dashed curve represents model prediction in water containing 8 ppm DO and a stress intensity value of 35 MPa·m$^{1/2}$.

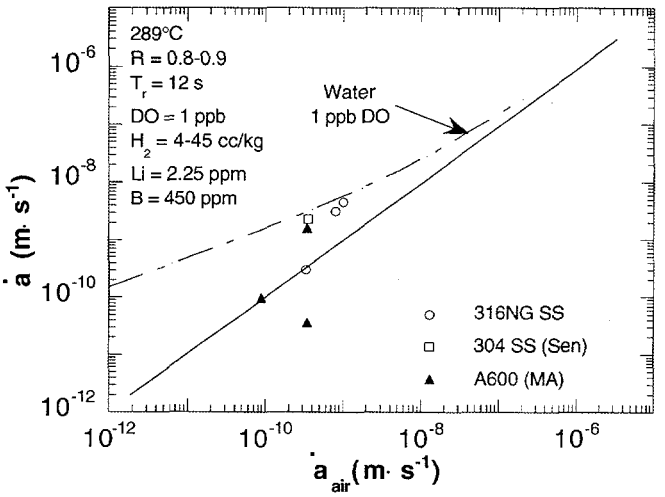

Figure 20.
Corrosion fatigue data for specimens of Alloy 600, Type 316NG and sensitized Type 304 SS in simulated PWR primary water at 289°C. Dashed line represents model predictions for austenitic SSs in water containing 1 ppb DO. Diagonal line corresponds to crack growth of SSs in air.

contribution from stress corrosion cracking in the low-oxygen environment. With the exception of one data point for the Alloy 600 specimen, the experimental results are bounded by the model prediction (dashed line) and the "air line" for austenitic SSs predicted by the ASME Code. Additional CGR data for austenitic SS specimens are required to validate model predictions in water containing low DO concentrations.

3.1.3 Morphology of Crack Path and Surface of Stainless Steel and Alloy 600 CGR Specimens

The morphology of corrosion-fatigue cracks in the Alloy 600 and austenitic SS specimens listed in Tables 8 and 9 has been determined. The 1T-CT specimens were sectioned vertically, and one-half of each specimen was split in the plane of the crack in liquid nitrogen. The corrosion-product film was removed from the fracture surface by a chemical process to reveal the morphology of the underlying material. The intact portion of the specimen that encompassed the crack was polished and etched to corroborate the mode of crack propagation and also to determine if crack branching had occurred during

the test. The total crack lengths at the end of the test were compared with values obtained by the DC potential–drop technique.

Figures 21–26 show the fracture surface, fracture morphology, and crack path in the crack–tip region of the specimens. The crack path and fracture morphology of the sensitized Type 304 SS specimens indicated a predominantly intergranular mode of crack propagation in oxygenated water (Figs. 21 and 22). The Alloy 600 specimen, which has a very small grain size, also exhibited intergranular cracking in this environment (Fig. 23). The crack path in specimens in which the environment at the beginning and end of the experiment was simulated primary PWR, with an intermediate period of oxygenated HP water, revealed transgranular cracking in the Alloy 600 specimen under all conditions (Fig 24). The Type 316NG (Fig. 25) and sensitized Type 304 SS (Fig. 26) specimens also exhibited a transgranular mode of crack propagation during tests in simulated PWR water and in oxygenated HP water. Intergranular cracking of the sensitized Type 304 SS specimen in oxygenated water was not observed because of the low load ratio in most of the tests.

TYPE 304 SS	HEAT TREATMENT	LOAD CONDITIONS	ENVIRONMENT
Spec. No. C–34 Heat No. 10285	1050°C for 0.5h plus 650°C for 2 h	K_{max} = 30–41 MPa·m$^{1/2}$ R = 0.60–0.95 Freq. = 0.077 Hz	200–300 ppb DO 0–200 ppb Chromate 0–100 ppb Sulfate

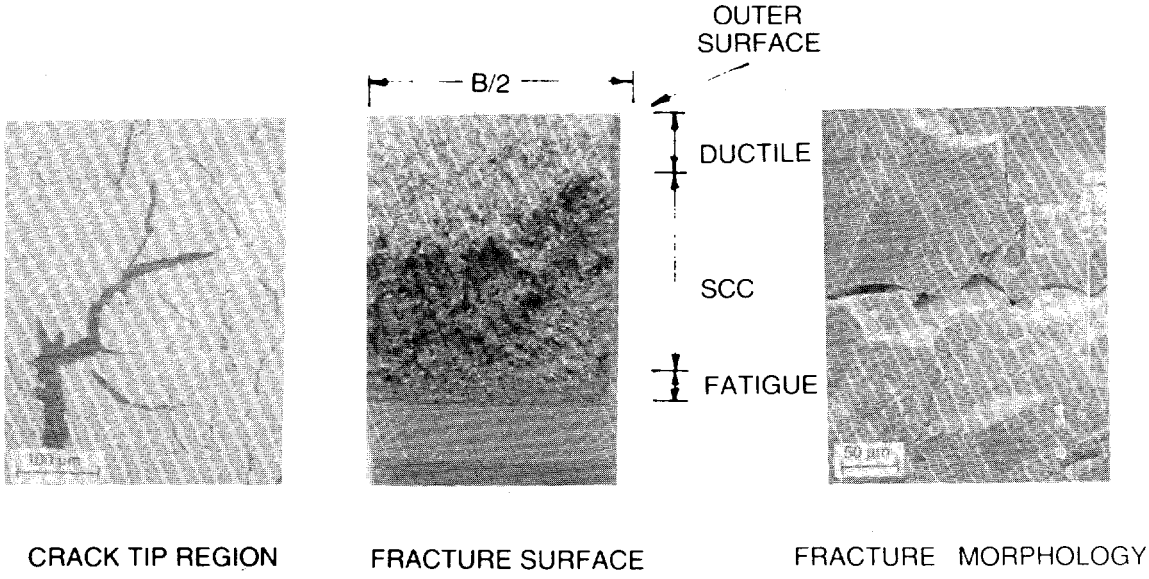

Figure 21. Crack path, fracture surface, and fracture morphology of 1T–CT specimen of Type 304 SS (No. C–34) after crack growth experiment in oxygenated HP water and oxygenated water containing chromate, sulfate, 2–butanone–oxime, or ethanolamine at 289°C

TYPE 304 SS	HEAT TREATMENT	LOAD CONDITIONS	ENVIRONMENT
Spec. No. C-35 Heat No. 10285	1050°C for 0.5h plus 650°C for 8 h	K_{max} = 31-39 MPa·m$^{1/2}$ R = 0.60-0.95 Freq. = 0.077 Hz	200-300 ppb DO 0-200 ppb Chromate 0-100 ppb Sulfate

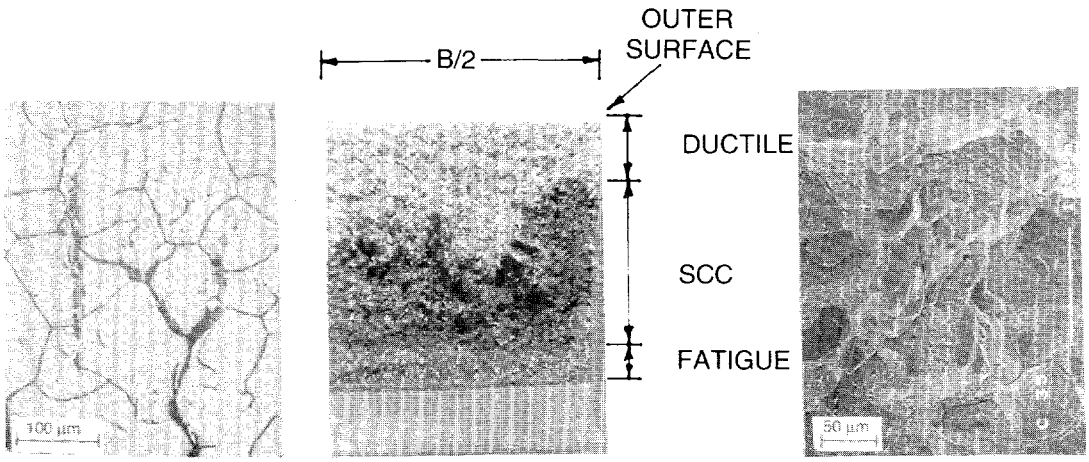

Figure 22. Crack path, fracture surface, and fracture morphology of 1T-CT specimen of Type 304 SS (No. C-35) after crack growth experiment in oxygenated HP water and oxygenated water containing chromate, sulfate, 2-butanone-oxime, or ethanolamine at 289°C

ALLOY 600	HEAT TREATMENT	LOAD CONDITIONS	ENVIRONMENT
Spec. No. IN-1 Heat No. J422	As-received Mill annealed	K_{max} = 28-396MPa·m$^{1/2}$ R = 0.60-0.95 Freq. = 0.077 Hz	200-300 ppb DO 0-200 ppb Chromate 0-100 ppb Sulfate

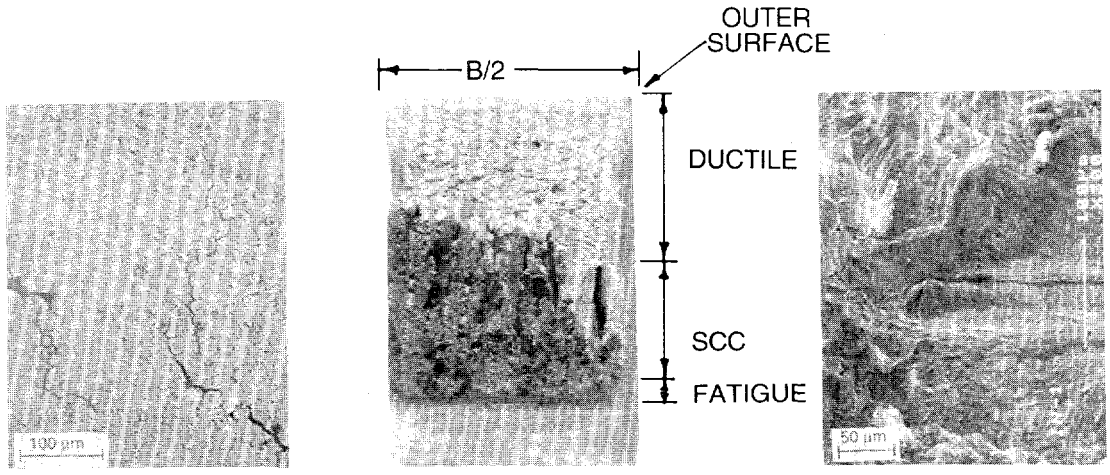

Figure 23. Crack path, fracture surface, and fracture morphology of 1T-CT specimen of Alloy 600 (No. IN-1) after crack growth experiment in oxygenated HP water and oxygenated water containing chromate, sulfate, 2-butanone-oxime, or ethanolamine at 289°C

ALLOY 600	HEAT TREATMENT	LOAD CONDITIONS	ENVIRONMENT
Spec. No. IN–2 Heat No. J422	As-received Mill annealed	K_{max} = 29–31 MPa·m$^{1/2}$ R = 0.2–1.0 Freq. = 0.077 Hz at R <1.0	HP Water; 6 ppm DO and PWR Water; 450 ppm B, 2.25 ppm Li, 4–45 cc/kg H_2

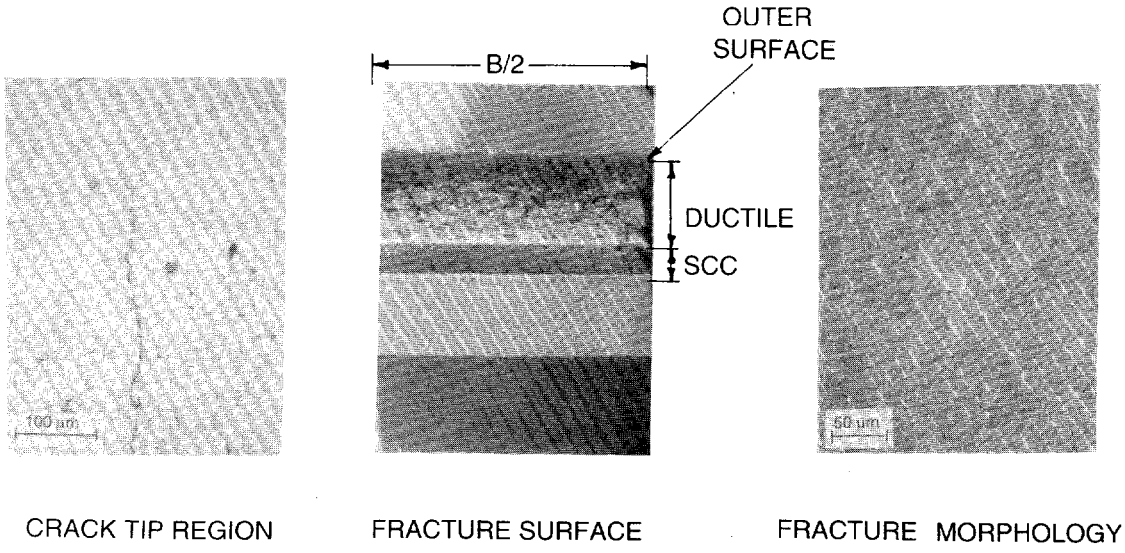

Figure 24. Crack path, fracture surface, and fracture morphology of 1T–CT specimen of Alloy 600 (No. IN–2) after crack growth experiment in HP water and simulated PWR water at 289°C

TYPE 316NG SS	HEAT TREATMENT	LOAD CONDITIONS	ENVIRONMENT
Spec. No. 198–2 Heat No. 13198	1050°C for 0.5h plus 650°C for 24 h	K_{max} = 30–43 MPa·m$^{1/2}$ R = 0.2–1.0 Freq. = 0.077 Hz at R <1.0	HP Water; 6 ppm DO and PWR Water; 450 ppm B, 2.25 ppm Li, 4–45 cc/kg H_2

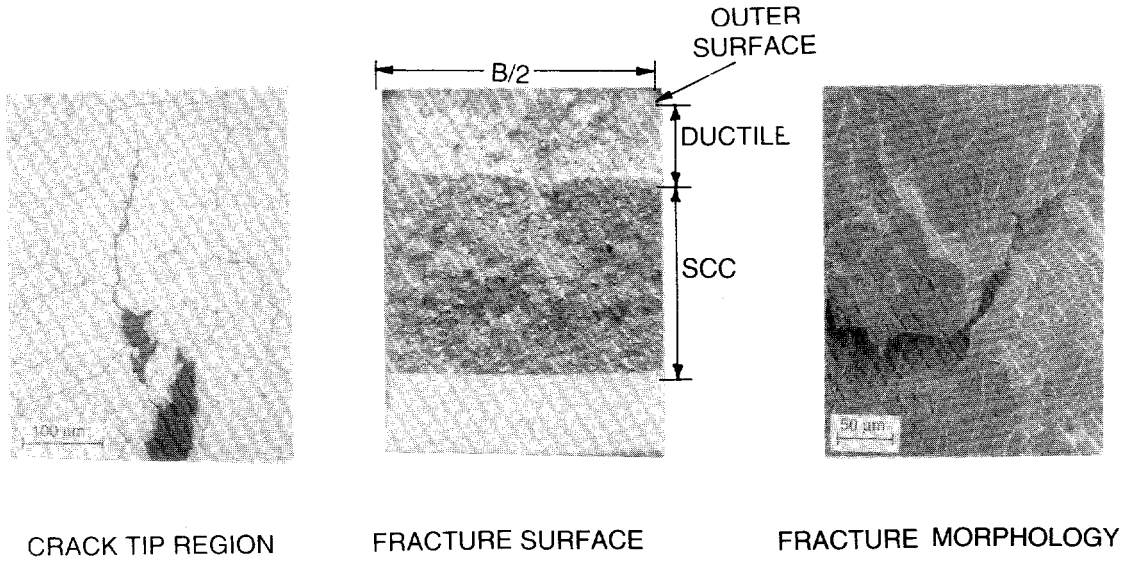

Figure 25. Crack path, fracture surface, and fracture morphology of 1T–CT specimen of Type 316NG SS (No. CTD–198–02) after crack growth experiment in HP water and simulated PWR water at 289°C

TYPE 304 SS	HEAT TREATMENT	LOAD CONDITIONS	ENVIRONMENT
Spec. No. 37 Heat No. 30956	1050°C for 0.5h plus 700°C for 12 h	K_{max} = 31–40 MPa·m$^{1/2}$ R = 0.2–1.0 Freq. = 0.077 Hz at R <1.0	HP Water; 6 ppm DO and PWR Water; 450 ppm B, 2.25 ppm Li, 4–45 cc/kg H_2

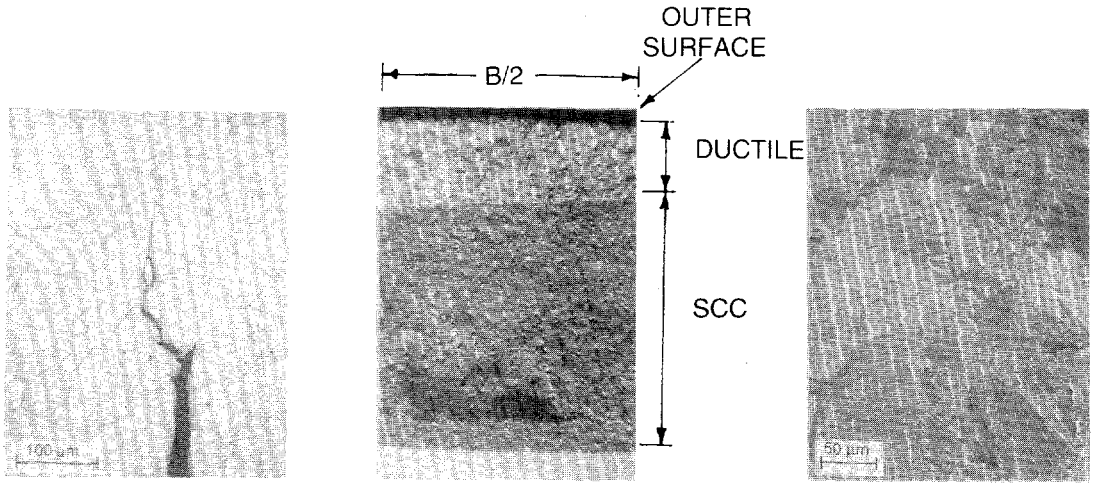

Figure 26. Crack path, fracture surface, and fracture morphology of 1T–CT specimen of Type 304 SS (No. 37) after crack growth experiment in HP water and simulated PWR water at 289°C

4 Irradiation-Assisted SCC of Austenitic SSs

In recent years, failures of reactor–core internal components in both BWRs and PWRs have increased after accumulation of relatively high fluence (>5 x 10^{20} n·cm^{-2}, E >1 MeV). The general pattern of the observed failures indicates that as nuclear plants age and neutron fluence increases, various apparently nonsensitized austenitic SSs become susceptible to intergranular failure. Some components (e.g., BWR dry tubes, control blade handle and sheath) are known to have cracked under minimal applied stress. Although most failed components can be replaced, some safety–significant structural components (e.g., BWR top guide, shroud, and core plate) would be very difficult or impractical to replace. Therefore, the structural integrity of these components after accumulation of high fluence has been a subject of concern, and extensive research has been conducted to provide an understanding of this type of degradation, which is commonly known as irradiation–assisted stress corrosion cracking (IASCC).

In the mid-1960s, investigators began to implicate impurities such as Si, P, and S in IASCC failure of components fabricated from solution-annealed nonsensitized austenitic SS. However, in direct contradiction of the earlier beliefs and initially encouraging test results obtained from high–purity (HP) Type 348 austenitic SSs, several investigators in recent years have reported results from slow–strain–rate–tensile (SSRT) and in–reactor tests that indicate resistance of HP heats (low in Si, C, P, and S) of Type 304 and 348 SS to IASCC failure is no better than that of commercial–purity (CP) materials. Therefore,

the issue of superior performance of HP materials and the mechanisms of IASCC appear to be far from established.

In general, heat-to-heat variation in susceptibility to IASCC has been observed to be very significant regardless of material grade, even among similar HP materials containing virtually identical chemical composition. This seems to cast serious doubt not only on the role of grain-boundary segregation of impurities (i.e., Si, P, or S) but also on the premise that Cr depletion is the only important mechanism of IASCC. Although grain-boundary Cr depletion is believed by most investigators to play a role, it has been suspected that there may be other important mechanisms of IASCC of solution-annealed materials associated with impurity elements (e.g., trace impurities) that are not specified in the ASTM specifications and that have been overlooked by most investigators. Such trace impurities could be associated with iron and steel-making processes and with fabrication and welding of the actual reactor components. Other mechanisms have also been proposed. Some investigators suspect that hydrogen plays an important role through a yet-to-be-identified synergism in the process of IASCC, and other investigators suspect that the degree of metastability of various heats of austenitic SS plays an important role via other unidentified processes.

In the present reporting period, our primary effort has been focused on determining the effects of water chemistry on susceptibility to IASCC of specimens from BWR components. Progress was also made in assembly and calibration of a J-R test facility that will be used to determine fracture toughness of the compact-tension specimens being irradiated in the Halden reactor, Norway.

4.1 Effects of Water Chemistry on SCC of Irradiated Austenitic Stainless Steels (H. M. Chung, W. E. Ruther, and A. G. Hins)

4.1.1 Introduction

Probably the most important factor that many investigators believe lends support to a Cr-depletion mechanism for IASCC is the observation that the dependence of IGSCC of nonirradiated thermally sensitized material and IASCC of irradiated solution-annealed material on water chemistry, namely DO, is similar (e.g., see Ref. 36). However, the data base on effects of DO on IASCC is rather limited, and only a few investigations have been reported in the literature for BWR-irradiated materials.[37-39] Results from a limited number of SSRT tests appear to indicate that the threshold electrochemical potential (ECP) of SSs in high-temperature water and DO necessary to protect against IASCC is <-140 mV SHE[37] and <0.01 ppm,[38,39] respectively, for CP-grade Type 304 SS. Results from uniaxial constant-load tests reported by Katsura et al.[40] are also consistent with SSRT data. However, similar tests by Jenssen and Ljungberg[41] on rod tensile specimens fabricated from numerous CP and HP heats of Type 304 and 316 SS and irradiated in a BWR indicate significant heat-to-heat variations in susceptibility to IASCC and in its dependence on water chemistry. We have reported similar behavior for specimens from several HP and CP heats of Type 304 SS irradiated in BWRs for a single water chemistry, i.e., ≈0.3 ppm DO and an ECP of ≈60-150 mV SHE.[42,43,*] In this report, the effects of

* H. M. Chung, W. E. Ruther, J. E. Sanecki, and T. F. Kassner, *Role of Trace Elements in Stress Corrosion Cracking of Irradiated Austenitic Stainless Steels*, Presented at Proc. 17th Symp. on Effects of Radiation on Materials, Sun Valley, ID, June 20-23, 1994.

water chemistry were investigated for a wider range of DO and ECP. The objective was twofold: (1) to better define the effects of water chemistry on susceptibility of the HP and CP Type 304 SS BWR components to IG cracking, thereby providing an independent confirmation of the protection potential; and (2) to obtain insight into the origin of heat-to-heat variations in susceptibility to IASCC.

4.1.2 Experimental Procedures

Materials and Irradiation. A description of the hot-cell SSRT tests was given in a previous report.[42] Cylindrical SSRT specimens 89-mm long were sectioned from top-, middle-, and bottom-axial positions of BWR neutron-absorber rods listed in Table 10. Boron carbide was removed by drilling. Maximum fluence at the top was determined from known in-reactor flux data. Lower fluences at the other two axial locations were determined from results of ^{60}Co gamma scans of the entire length of the rods. Sheet tensile specimens (57.2-mm long, 12.7-mm wide, and 1.22-mm thick), fabricated from BWR control-blade sheaths, were also tested. The sheath specimens had a gage section ≈19.1-mm long and 3.2-mm wide.

The fast-neutron fluence and chemical composition of three HP and two CP heats of Type 304 SS are also given in Table 10. Documentation of chemical composition of the CP-grade neutron absorber and control-blade sheath were not available from either the utility or the reactor-fuel supplier. The fast (E >1 MeV) neutron fluence of the HP and CP neutron-absorber tube specimens, irradiated in four different BWRs (Table 10), ranged from $0.2 \times 10^{21} - 2.6 \times 10^{21}$ n·cm^{-2}.

Table 10. Chemical composition (in wt.%) and fluence of high- and commercial-purity Type 304 SS BWR components

Heat ID No.	Cr	Ni	Mn	C	N	B	Si	P	S	Source Code	Service Reactor	Fluence (10^{21} n·cm^{-2})
HP304-A	18.50	9.45	1.53	0.018	0.100	<0.001	<0.03	0.005	0.003	NAT[a]	BWR-B	0.2-1.4
HP304-B	18.30	9.75	1.32	0.015	0.080	<0.001	0.05	0.005	0.005	NAT[a]	BWR-B	0.2-1.4
HP304-CD	18.58	9.44	1.22	0.017	0.037	0.001	0.02	0.002	0.003	NAT[a]	BWR-B	0.2-1.4
HP304-CD	18.58	9.44	1.22	0.017	0.037	0.001	0.02	0.002	0.003	NAT[a]	BWR-QC	2.0
CP304-A	16.80	8.77	1.65	0.08[b]	0.052	-	1.55	0.045[b]	0.030[b]	NAT[c]	BWR-Y	0.2-2.0
CP304-B	18-20	8-10.5	2.00[b]	0.08[b]	-	-	1.00[b]	0.045[b]	0.030[b]	CBS[d]	BWR-LC	0.5-2.6

[a]High-purity neutron absorber tubes, OD=4.78 mm, wall thickness = 0.63 mm, composition before irradiation.
[b]Represents maximum value in the specification; actual value not measured.
[c]Commercial-purity absorber tubes, OD = 4.78 mm, wall thickness = 0.79 mm, composition after irradiation.
[d]Commercial-purity control blade sheath, thickness 1.22 mm, actual composition not measured.

SSRT Test Results. SSRT tests were conducted in air (Table 11) and in simulated BWR water (Tables 12 and 13) at 289°C at a fixed strain rate of 1.65×10^{-7} s^{-1}. SSRT tests in water were conducted at DO concentrations of ≈8 ppm (Table 12) and ≈0.3 ppm (Table 13). Conductivity of the water was ≈0.12 μS·cm^{-1} for tests with 0.3-8 ppm DO. Dissolved oxygen content in water was established by purging deaerated HP feedwater with a nitrogen/oxygen gas mixture and maintaining the cover gas at a specified pressure. Effluent DO was determined by Chemetric™ measurements, and ECP values of Type 304 SS and platinum electrodes were obtained versus an external 0.1M KCl/AgCl/Ag reference electrode located at the outlet of the autoclave. A SSRT test was initiated when the ECP of SS stabilized; ECP was measured periodically until the

specimen fractured. For most of the tests, ECP remained fairly constant; however, a gradual increase in ECP (as much as ≈30%) occurred in some experiments. The DO, average ECP, conductivity, and pH of water for each SSRT test are listed in Tables 12 and 13.

Table 11. Results of tensile tests in air[a] on irradiated Type 304 SS BWR core-internal components at 289°C

Specimen Ident. No.	Hot-cell Ident. No.	Source Heat[b] Ident. No.	Fast-Neutron Fluence, $n \cdot cm^{-2}$	SSRT No.	Tensile Properties: Failure Time, h	Max. Stress, MPa	Yield Stress, MPa	Total Elong., %	%IG %
BL-BWR-2H	389E3A	CP304-A	2.0×10^{21}	IR-9	228	631	595	13.5	0
BL-BWR-2M	389E2D	CP304-A	0.6×10^{21}	IR-3	580	465	221	34.8	0
BL-BWR-2L	389E1A	CP304-A	0.2×10^{21}	IR-2	260	390	184	15.6	0
VH-A7A-L2	406A1F	HP304-A	1.4×10^{21}	IR-5	93	786	702	5.6	0
VM-D5B-L2	406C3	HP304-CD	0.7×10^{21}	IR-6	405	684	591	24.2	0
VL-A4C-L2	406B3	HP304-A	0.2×10^{21}	IR-10	231	607	460	13.7	0
C71U	LSC-1	CP304-B	2.45×10^{21}	IR-15	123	830	820	7.3	0
C72T	LCS-4	CP304-B	2.54×10^{21}	IR-13	121	876	815	7.2	0
C7T1T	LSC-7	CP304-B	1.59×10^{21}	IR-19	203	792	666	12.0	0
C7T1M7	LCS-9	CP304-B	1.17×10^{21}	IR-21	136	777	736	7.5	0
C7M2K	LSC-11	CP304-B	0.53×10^{21}	IR-23	361	644	570	21.4	0
C7B1W	LCS-5	CP304-B	0.23×10^{21}	IR-17	574	577	360	34.1	0

[a]In air at 289°C and strain rate of 1.65×10^{-7} s^{-1}.

Post-Test Examination. Analysis of the fracture surface of SSRT specimens was conducted by scanning electron microscopy (SEM) to determine quantitatively the fraction of intergranular fracture morphology (% IGSCC). Fractography by SEM was conducted at magnifications of 60–125X, and an entire fracture-surface composite was constructed for each specimen to determine the fractions of intergranular, transgranular, and ductile failure. Grain-boundary microchemistry was analyzed with a JEOL Company JAMP-10 Model scanning Auger microscope (SAM) on specimens charged with hydrogen and fractured in-situ in the ultrahigh vacuum of the SAM.[42,43,*]

Stress-Strain Behavior. For specimens in which neutron fluence, test temperature, strain rate, and DO were similar, the load-elongation curves were remarkably reproducible for a given heat of steel. This is shown in Fig. 27 for three HP heats of Type 304 SS irradiated to a fluence of $\approx 1.4 \times 10^{21}$ $n \cdot cm^{-2}$.

Figure 28 shows the percent IGSCC determined from SEM fractography as a function of total elongation in water from data in Tables 11–13. The figure shows that uniaxial ductility is an approximate measure of susceptibility to IGSCC (or vice versa) regardless of water chemistry (DO, ECP, pH, and conductivity). However, results of the present

* H. M. Chung, W. E. Ruther, J. E. Sanecki, and T. F. Kassner, *Role of Trace Elements in Stress Corrosion Cracking of Irradiated Austenitic Stainless Steels*, Presented at Proc. 17th Symp. on Effects of Radiation on Materials, Sun Valley, ID, June 20-23, 1994.

Table 12. SSRT[a] test results on irradiated HP and CP Type 304 SS BWR neutron-absorber tubes in HP water containing ≈8 ppm DO at 289°C

Source Heat Ident. No.	Fast-Neutron Fluence, $n \cdot cm^{-2}$	α-γ Hot Cell Ident. No.	Swagelok Ident. No.	SSRT No.	Feedwater Chemistry: Oxygen Conc., ppm	Feedwater Chemistry: Average ECP mV SHE	Feedwater Chemistry: Cond. at 25°C $\mu S \cdot cm^{-1}$	Feedwater Chemistry: pH at 25°C	SSRT Parameters: Failure Time, h	SSRT Parameters: Max. Stress, MPa	SSRT Parameters: Total Elong., %	SSRT Parameters: TGSCC %	SSRT Parameters: IGSCC %
HP304-A	1.4×10^{21}	A6A2-1	32	IR-41	8.3	+156	0.120	6.35	31.9	414	1.90	2	56
HP304-A	1.4×10^{21}	A6A2-2	33	IR-42	8.2	+267	0.118	6.48	31.9	372	1.89	3	68
HP304-B	1.4×10^{21}	473A-1	47	IR-43	8.9	+165	0.118	6.49	31.8	453	1.88	0	59
HP304-CD	1.4×10^{21}	473C-1	42	IR-44	8.2	+122	0.084	6.80	29.2	360	1.73	3	62
HP304-B	0.7×10^{21}	473D-1	38	IR-53	8.2	+155	0.119	6.49	55.8	445	3.3	-	-
CP304-A	0.2×10^{21}	389C1-1	28	IR-51	8.0	+164	0.098	6.09	153.0	310	9.1	47	0
CP304-A	0.6×10^{21}	389C2-1	20	IR-45	8.2	+131	0.083	6.80	154.3	359	9.2	55	2
CP304-A	2.0×10^{21}	389C3-2	27	IR-52	7.9	+178	0.066	7.06	43.5	390	2.6	3	52

[a]Strain rate of 1.65×10^{-7} s^{-1}.

Table 13. SSRT[a] test results on irradiated Type 304 SS specimens from BWR core-internal components in simulated BWR water containing ≈0.3 ppm DO at 289°C

Source Heat Ident. No.	Fast-Neutron Fluence, $n \cdot cm^{-2}$	α-γ Hot Cell Ident. No.	Specimen Ident. No.	SSRT No.	Feedwater Chemistry: Oxygen Conc., ppb	Feedwater Chemistry: Average ECP, mV SHE	Feedwater Chemistry: Cond. at 25°C $\mu S \cdot cm^{-1}$	Feedwater Chemistry: pH at 25°C	SSRT Parameters: Failure Time, h	SSRT Parameters: Max. Stress, MPa	SSRT Parameters: Yield Stress, MPa	SSRT Parameters: Total Elong., %	SSRT Parameters: TGSCC, %	SSRT Parameters: IGSCC, %
CP304-A	2.0×10^{21}	389E3D	BL-BWR-2H	IR-12	300	90	0.13	6.27	21	415	401	1.2	8	28
CP304-A	0.6×10^{21}	389E2A	BL-BWR-2M	IR-8	290	76	0.15	6.32	140	359	230	8.3	55	0
CP304-A	0.2×10^{21}	389E1D	BL-BWR-2L	IR-1	280	115	0.13	6.23	107	337	210	6.7	43	0
HP304-A	1.4×10^{21}	406A1E	VH-A7A-L1	IR-4	280	106	0.10	6.28	11	417	420	0.6	2	58
HP304-CD	0.7×10^{21}	406C2	VM-D5B-L1	IR-7	280	148	0.12	6.26	31	552	532	1.8	8	34
HP304-A	0.2×10^{21}	406B2	VL-A4C-L1	IR-11	330	88	0.14	6.33	77	520	451	4.6	47	14
CP304-B	2.26×10^{21}	LSC-2	C71X	IR-16	310	-	0.12	6.23	74	841	824	4.2	2	3
CP304-B	2.64×10^{21}	LCS-3	C72S	IR-14	320	-	0.11	6.25	84	843	807	5.0	2	4
CP304-B	1.53×10^{21}	LCS-8	C7T1J	IR-20	360	-	0.11	6.22	101	872	780	6.1	3	6
CP304-B	1.15×10^{21}	LSC-10	C7T1M8	IR-22	360	-	0.11	6.28	79	815	803	4.7	5	4
CP304-B	0.50×10^{21}	LCS-12	C7M2L	IR-24	325	-	0.08	6.38	290	657	594	18.1	0	0
CP304-B	0.20×10^{21}	LSC-6	C7B1X	IR-18	310	-	0.11	6.24	457	572	355	27.1	8	0

[a]Strain rate of 1.65×10^{-7} s^{-1}.

investigation (on BWR neutron absorber tubes and control blade sheath) indicate that, for a comparable ductility, susceptibility to intergranular cracking is somewhat lower than that obtained on BWR dry tubes.[38,39,44]

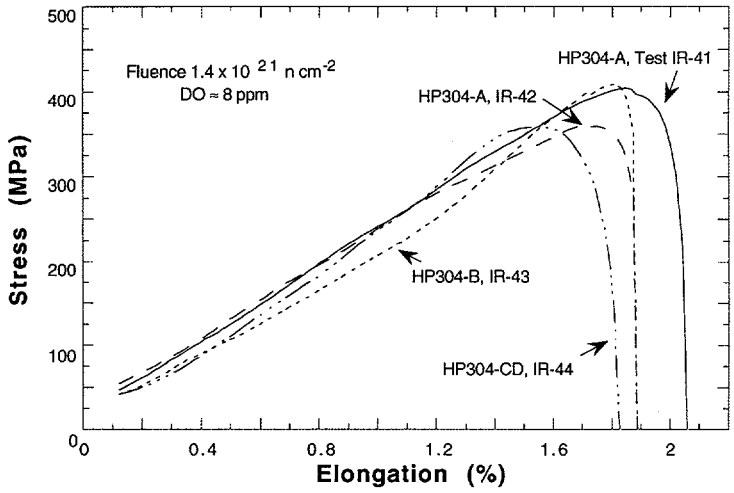

Figure 27. Load vs. elongation for specimens fabricated from neutron absorber tubes from three HP heats of Type 304 SS irradiated to 1.4 x 10^{21} n·cm^{-2} in BWRs

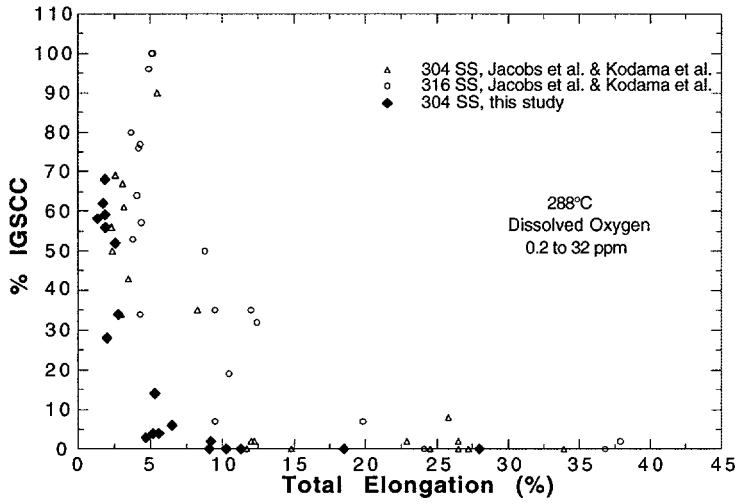

Figure 28. Total elongation vs. percent IGSCC for specimens fabricated from BWR-irradiated Type 304 and 316 SS determined in this and other investigations

Intergranular fracture morphology was observed only in specimens fractured in water; percent IGSCC was always zero or negligible for SSRT tests in air (Table 11). Nonductile fracture surface morphology resembling dislocation-channel-induced fracture was observed frequently in thin layers underneath the surface oxide either in air or water. This type of fracture will influence the nucleation of crack, but we believed it is irrelevant to the key process of intergranular cracking. This signifies the importance of the role of water as a corrosive environment in sustaining the grain-boundary separation. That is, the process is indeed stress corrosion cracking in nature but is not a mechanical process.

Susceptibility to IGSCC. The effect of DO on percent IGSCC vs. fluence is shown in Fig. 29 for HP (HP304-A, -B, and -CD) and CP (CP304-A) neutron absorber tubes in this study. Susceptibility of the control-blade sheath (fabricated from another CP-grade heat)

to IGSCC was negligible for all fluence levels; therefore, no tests were conducted to investigate the effect of DO, other than at ≈0.3 ppm. Percent IGSCC vs. DO (0.02–32 ppm) for CP Type 304 SS dry tubes, reported by Kodama et al.,[38,39] is also shown in Fig. 29 for comparison. The results obtained on BWR neutron–absorber and dry tubes fabricated from CP Type 304 SS appear to be quite similar considering the variations in fluence of the CP materials (≈1.3 x 10^{21} – 6.0 x 10^{21} n·cm^{-2}). Despite this range in fluence, susceptibility to IASCC seems to be determined primarily by DO and is relatively independent of fluence (>1.3 x 10^{21} n·cm^{-2}) at a given DO concentration.

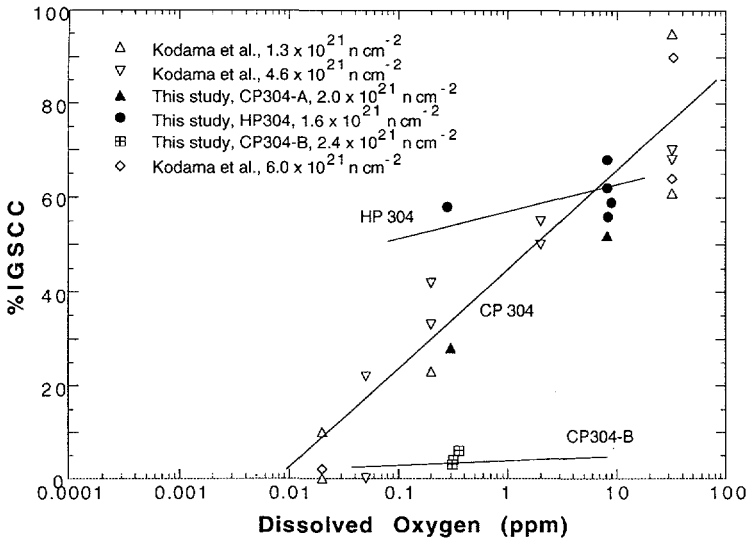

Figure 29. Percent IGSCC vs. DO for specimens of HP and CP Type 304 SS from neutron absorber tubes (this study) and CP Type 304 SS from dry tubes (Kodama et al.). Three distinct trends in DO dependence are evident.

The dependence of percent IGSCC on DO for neutron absorber tubes fabricated from HP Type 304 SS appears to be different from that of CP materials in several respects. For comparable fluence level, susceptibility of the former material to IGSCC seems to be less dependent on DO. Susceptibility of HP Type 304 SS seems to be significantly higher than CP grade regardless of DO and fluence.[42] Similar trends are also obvious from Fig. 30, in which percent IGSCC is plotted versus ECP from data obtained on specimens from BWR components irradiated to fluences of ≈1.4 x 10^{21} – 2.4 x 10^{21} n·cm^{-2}. In the figure, results obtained for CP Type 304 SS by Indig et al.[37] (sheet, fluence ≈1.9 x 10^{21} n·cm^{-2}) and in the present investigation (absorber tube, fluence ≈2.0 x 10^{21} n·cm^{-2}) appear to be comparable, whereas specimens from HP Type 304 SS absorber tubes exhibit cracking behavior relatively less sensitive to ECP than do the CP materials.

Crack Growth Rate. Approximate intergranular crack growth rates (CGRs) were estimated from SSRT data by a procedure similar to that of Jenssen and Ljungberg.[41] In the present study, CGR was estimated only for specimens in which through-wall IG cracks had been confirmed by SEM fractography. For such specimens, the depth and time of IG crack propagation can be determined fairly accurately from the fracture-surface map and load-elongation curve, respectively. The estimated CGRs determined in this way are listed in Table 14 and plotted as a function of ECP in Fig. 31. Also shown in the figure are similar results determined from the SSRT data reported by Jenssen and Ljungberg[41] and Kodama et al.[38,39] and constant-load test data reported by Katsura et al.[40] Figure 32 shows ECP of Type 304 SS as a function of effluent DO in HP water in our investigation.

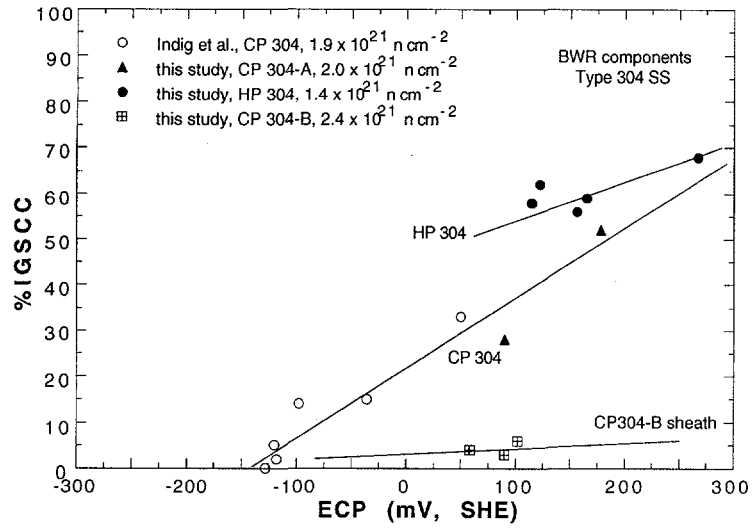

Figure 30. Percent IGSCC vs. ECP for HP and CP Type 304 SS specimens from neutron absorber tubes (this study) and from CP Type 304 SS sheet (Indig et al.)

Table 14. Intergranular crack growth rate estimated from SSRT tests on irradiated Type 304 and 316 SS BWR core-internal components in simulated BWR water at 289°C

Source Heat Ident. No.	Fast Neutron Fluence, n·cm^{-2}	SSRT No.	Feedwater Chemistry: Oxygen Conc., ppm	Feedwater Chemistry: Ave. ECP, mV SHE	SSRT Parameters: Failure Time, h	SSRT Parameters: IGSCC, %	SSRT Parameters: Max. IGSCC Penetration, %	SSRT Parameters: IGSCC Depth, mm	SSRT Parameters: Intergranular CGR, 10^{-8} m·s^{-1}
CP304-A[a]	2.0 x 10^{21}	IR-12	0.30	90	21.0	28	100	0.79	1.04
CP304-A	2.0 x 10^{21}	IR-52	7.9	178	43.5	52	100	0.79	0.51
HP304-A[b]	1.4 x 10^{21}	IR-4	0.28	106	11.2	58	100	0.63	1.56
HP304-CD	0.7 x 10^{21}	IR-7	0.28	148	31.0	34	100	0.63	0.56
HP304-A	1.4 x 10^{21}	IR-41	8.3	156	31.9	56	100	0.63	0.55
HP304-A	1.4 x 10^{21}	IR-42	8.2	267	31.9	68	100	0.63	0.55
HP304-B	1.4 x 10^{21}	IR-43	8.9	165	31.8	59	100	0.63	0.54
HP304-CD	1.4 x 10^{21}	IR-44	8.2	122	29.2	62	100	0.63	0.60

[a]Commercial-purity Type 304 SS, wall thickness 0.63 mm, tested at a strain rate of 1.65 x 10^{-7} s^{-1}.
[b]High-purity Type 304 SS, wall thickness 0.79 mm, tested at a strain rate of 1.65 x 10^{-7} s^{-1}.

Results in Fig. 31 indicate that CGRs estimated from SSRT and constant-load tests on specimens from BWR components are similar for a similar range of fluence and ECP. However, these CGRs (obtained from specimens sectioned from BWR components) are higher than those from the SSRT data reported by Jenssen and Ljungberg for BWR-irradiated rod-shape test specimens. In the latter investigation, strain rate was significantly lower (i.e., 5 x 10^{-8} s^{-1}) than that used by Kodama (2.5 x 10^{-7} s^{-1}) and in our investigation (1.7 x 10^{-7} s^{-1}). It is not clear if the higher CGRs of the reactor-component materials can be attributed to component fabrication variables, differences in irradiation conditions, or factors such as stress intensity and strain rate. Stress intensity is not likely to have been comparable in these tests, and a more accurate comparison would be possible if CGRs were obtained under conditions of constant stress intensity.

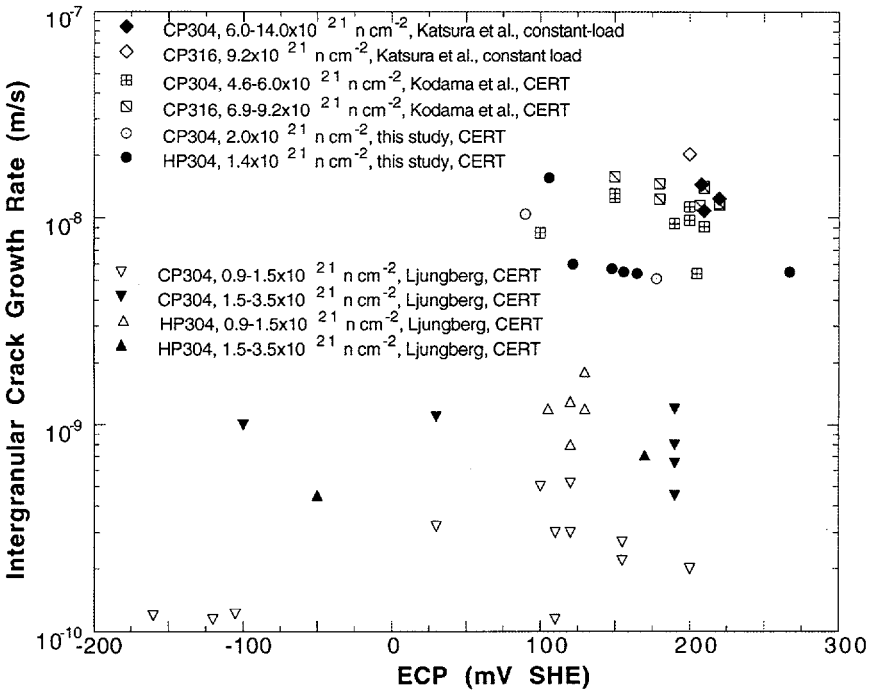

Figure 31. Intergranular crack growth rate of irradiated Type 304 and 316 SS at 289°C vs. ECP of simulated BWR water estimated from SSRT and constant-load tests on specimens from BWR neutron-absorber and dry tubes and rod-tensile specimens irradiated in BWRs

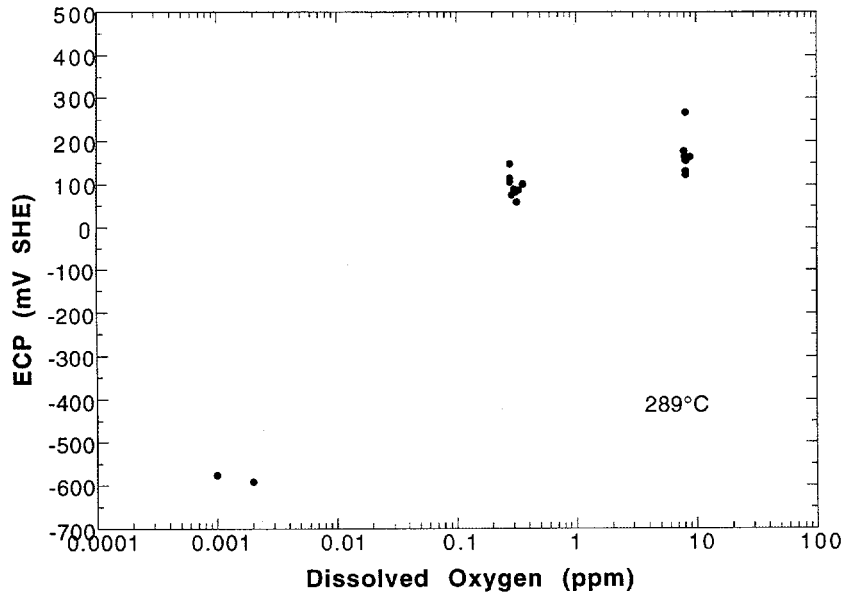

Figure 32. ECP of Type 304 SS versus effluent DO measured in this study

4.1.3 Discussion

We have reported previously that the HP-grade neutron-absorber tubes are characterized by more pronounced grain-boundary Cr depletion[42] and a higher level of fluorine contamination[45] than those of CP-grade absorber tubes or sheath. This difference may cause a higher susceptibility of the HP material to IASCC. The synergistic effect of a lower concentration of Cr and a higher concentration of fluorine on grain boundaries on percent IGSCC shown in Figs. 33 and 34, respectively, appears to be consistent with IGSCC results by Ward et al.[46] They reported fluorine-accelerated IGSCC of nonirradiated thermally sensitized bend specimens and weldments of CP-grade Type 304 SS that were contaminated with a fluorine-containing weld flux. Ward et al. reported that fluorine-assisted IGSCC was less sensitive to DO than was classical IGSCC of thermally sensitized fluorine-free specimens, which is consistent with our results (Fig. 29) on HP neutron-absorber tubes. However, a mechanistic understanding of the fluorine-assisted IGSCC and the strong influence of grain-boundary Cr depletion (via thermal sensitization in the case of the investigation by Ward et al.) have not been rationalized.

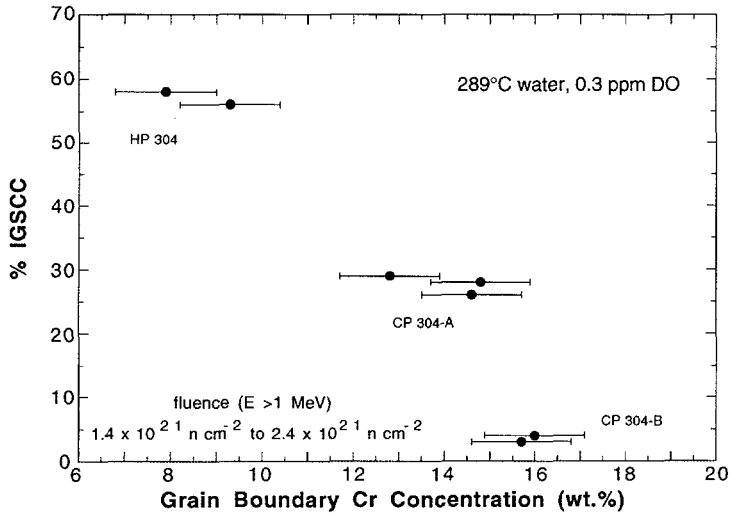

Figure 33.
Percent IGSCC at DO of ≈0.3 ppm for HP and CP Type 304 SS material irradiated in BWRs vs. grain-boundary Cr concentration determined by AES

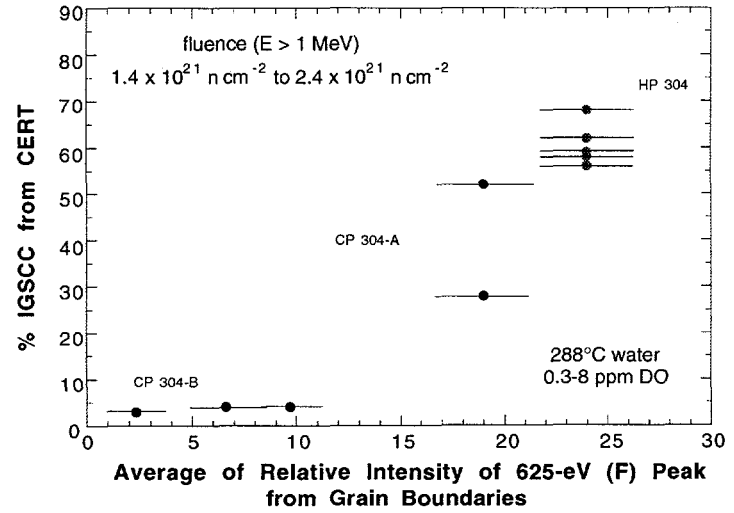

Figure 34.
Percent IGSCC vs. average intensity of fluorine signal from grain boundaries of HP and CP Type 304 SS material irradiated in BWRs

Halide impurities play a catalytic role in accelerating aqueous corrosion of Fe and Fe-base alloys but their influence can be strongly mitigated by the concentration of Cr ions in water.[47] The corrosion acceleration has been attributed to the rate of formation of ligand complex between Fe-halide (i.e., halide anion chemisorbed on Fe) and H_2O molecules, which has a rate several orders of magnitude higher than that of a similar ligand complex between halide-free Fe atoms and H_2O molecules.[47] A similar effect can be postulated for relative reaction rates to form fluorine-containing and fluorine-free ligand complexes of $FeF(H_2O)_5$ and $Fe(H_2O)_6$, respectively. A halide atom is released from the labile ligand complex [e.g., $FeF(H_2O)_5$] dissolved in water when H_2O replaces the halide atom in the complex, thus leading to a classical catalysis by halides. However, this reaction chain is broken when the concentration of Cr ions in water is high (e.g., at a crack tip in which grain boundaries exhibit minimal Cr depletion), because Cr-halide-H_2O ligand complex [e.g., $CrF(H_2O)_5$] forms rapidly but remains inert in water. This inhibits a catalytic role of the halide atoms (e.g., fluorine atoms). According to this model, several key factors that could influence susceptibility to IASCC are the concentration of free halide atoms (e.g., fluorine) available on grain boundaries (i.e., those not trapped by stable precipitates[45] or compounds), the concentration of Cr ions in water at the crack tip, and the lability of $FeF_x(H_2O)_y$ complex under irradiation in LWR water.

The above hypothesis seems to be consistent not only with the behavior of HP-grade neutron-absorber tubes (high susceptibility) and CP-grade control-blade sheath (negligible susceptibility) observed in our study but also with increased susceptibility to IGSCC of fluorine-contaminated welds of either nonirradiated or irradiated Type 304 SS. However, it is too early to make a conclusive statement regarding its validity and applicability to cracking of LWR core-internal components. Nonetheless, irradiation-induced grain-boundary depletion of Cr and contamination and segregation of halides (most likely fluorine) during component fabrication appear to be the two key processes that may produce synergistic effects leading to increased susceptibility to IASCC. Compared to nonirradiated and solution-annealed material, the synergistic effect will be undoubtedly more pronounced for materials in which yielding in grain matrix is relatively more difficult as a result of hardening by either irradiation or cold work.

4.2 Development of Hot-Cell J-R Test Facility (T. H. Hughes and E. E. Gruber)

Detailed design work for the J-R test apparatus has been completed, and several components have been received. Components for the load frame, load train, and mounting hardware for the furnace and hydraulic actuator have been fabricated. The load cell and the actuator for the J-R test system has been received. The furnace has been modified to allow attachment of an air cylinder, for remote positioning. The furnace shell has also been strengthened internally to enable temporary support of the upper test assembly. The air cylinder will be used to raise and lower the assembly during transfer into and out of the cell. The test assembly will be locked in the raised position during testing. The test train components have been fabricated; these components include the upper and lower test cages, clevis holders, Zircaloy pins, and clevises. The actuator and hydraulic system has been installed. The electronic control system has been connected and tested by Instron Corporation technical support personnel. The position LVDT has also been calibrated by Instron, and the load cell is being calibrated with the use of a

standard at Argonne National Laboratory. Work is in progress to align the load train and develop a LabVIEW™ data acquisition program.

Six dummy specimens with the same geometry as the compact-tension specimens being irradiated in the Halden reactor have been fabricated from nonirradiated Type 302 SS. These specimens will be used for preliminary testing and calibration of the apparatus. Similar sets of specimens will be fabricated from actual archive materials of the 27 heats of SS being irradiated in the Halden reactor to obtain baseline J-R properties in nonirradiated condition.

5 Summary of Results

5.1 Fatigue of Ferritic Steels

Fatigue behavior of A106-Gr B carbon steel and A533-Gr B and A302-Gr B low-alloy steels has been investigated in air and water environments. The results confirm the significant reduction in fatigue life in high-DO water and strong dependence on strain rate. The results show that although the structure and cyclic-hardening behavior of carbon and low-alloy steels are distinctly different, there is little or no difference in susceptibility to environmental degradation of fatigue life of these steels, when sulfur levels are comparable. The A106-Gr B and A302-Gr B steels exhibit dynamic strain-aging, whereas strain-aging effects are modest in the A533-Gr B low-alloy steel.

In an air environment, the fatigue life of low-alloy steels is greater than that of the carbon steel, and strain rate has little or no effect on fatigue life of A106-Gr B and A533-Gr B steels in air. The results for A302-Gr B steel indicate a possible effect of strain rate on fatigue life.

For both carbon and low-alloy steels, the results indicate only a marginal effect of simulated PWR environment on fatigue life, e.g., fatigue life is lower by less than a factor of 2 than that in air. Furthermore, fatigue life is independent of strain rate; a three-order-of-magnitude decrease in strain rate does not cause an additional decrease in life. The results also indicate that the modest decreases of fatigue life in simulated PWR water are valid for high-sulfur steels (e.g., A302-Gr B steel with 0.027 wt.% sulfur) that exhibit enhanced crack growth rates in precracked specimens.

Environmental effects on fatigue life are significant at high DO levels, e.g., 0.5-0.8 ppm DO. For high-DO water, the effects of various loading and environmental parameters on fatigue life of carbon and low-alloy steels are summarized below.

(i) The fatigue life of carbon and low-alloy steels decreases rapidly with decreasing strain rate. For both steels, the effect of strain rate saturates at ≈0.001%/s. Compared with tests in air, fatigue life of A106-Gr B steel in high-DO water is lower by factors of 2, 4, 10, and 18 at strain rates of 0.4, 0.04, 0.004, and 0.0004%/s, respectively. A further decrease in strain rate by one order of magnitude does not cause additional decrease in fatigue life.

(ii) A minimum strain is required for environmentally assisted decrease in fatigue life. For the loading conditions used in the present study, this threshold strain range appears to be ≈0.36% for the heats of carbon and low-alloy steels investigated.

(iii) A slow strain rate applied during the tensile-loading cycle is more effective in environmentally assisted reduction in fatigue life than when applied during the compressive-loading cycle. Also, a slow strain rate applied during both the compressive- and the tensile-loading cycles does not cause further decrease in fatigue life.

(iv) The results also indicate that a slow strain rate applied during each portion of the tensile-loading cycle above the threshold strain is equally effective in decreasing fatigue life.

(v) A hold period at peak tensile strain decreases fatigue life in high-DO water but not in air. A 5-min hold is sufficient to reduce fatigue life.

(vi) A detailed metallographic examination of the test specimens and exploratory tests indicate that the reduction in fatigue life in high-DO water is primarily due to environmental effects on fatigue crack propagation. Environment appears to have little or no effect on crack nucleation. Although all specimens tested in water show surface micropitting, there is no indication that these micropits enhance crack nucleation. Irrespective of environment, cracks in carbon and low-alloy steels nucleate either along slip bands, carbide particles, or at the ferrite/pearlite phase boundaries.

5.2 Environmentally Assisted Cracking of Alloy 600 and Wrought SSs in Simulated LWR Water

Fracture-mechanics CGR tests were conducted on compact-tension specimens of sensitized Type 304, Type 316NG, and mill-annealed Alloy 600 in oxygenated water and in deaerated water containing B, Li, and dissolved H_2 at low concentrations at 289°C. Tests on mill-annealed Alloy 600 and two sensitized Type 304 SS specimens in simulated BWR water (≈200 ppb DO at conductivities of ≈0.08 to 8.3 $\mu S \cdot cm^{-1}$) indicated that Alloy 600 and sensitized Type 304 SS had virtually the same CGRs under conditions where EAC occurs in both materials, i.e., when the stress intensity exceeds a threshold value at a given load ratio. Experimental data for the three specimens were compared with predictions from an Argonne National Laboratory (ANL) model for CGRs of SSs in water[33] and the ASME Section XI correlation for CGRs in air at the K_{max} and load-ratio values in the various tests. The data for both materials were bounded by the two curves.

The effect of water chemistry on CGRs of the materials was explored at a load ratio of 0.95. Small amounts of chromate and sulfate (<200 ppb) and two amines (1-5 ppm) in water that contained ≈200 ppb DO produced small but measurable changes in the CGRs of the sensitized Type 304 SS specimens but had virtually no effect on the CGR of the mill-annealed Alloy 600 specimen. The average CGR of the Alloy 600 and sensitized Type 304 SS specimens was ≈2.3 x 10^{-10} $m \cdot s^{-1}$ at an R of 0.95 and K_{max} of >30 $MPa \cdot m^{1/2}$ under these water chemistry conditions. This average rate is consistent with numerous determinations of EAC of sensitized Type 304 and nonsensitized Type 316NG SS

specimens in oxygenated water at 289°C under similar loading conditions.[34] The observation that different materials, e.g., Alloy 600, sensitized Type 304, nonsensitized Type 316NG, and CF-3, CF-8 and CF-8M grades of cast SSs,[35] exhibit the same CGR in oxygenated water, despite significant differences in material chemistry, microstructure, and mode of crack propagation, suggests that crack propagation is controlled by the rate of cathodic reduction of DO with a concomitant anodic dissolution process at the crack tip.

The crack growth behavior of Alloy 600, Type 316NG, and sensitized Type 304 SS was investigated in simulated PWR water at high load ratios where an environmental contribution to cracking may be significant. The tests were conducted at 289°C in water containing 450 ppm B and 2.25 ppm Li (added to the feedwater as H_3BO_3 and LiOH), 4–45 $cm^3 \cdot kg^{-1}$ H_2, ≈1 ppb DO, and 750 ppb hydrazine. The CGR data for the specimens were compared with predictions from the ANL crack-growth model that was modified to account for a very low DO concentration in simulated PWR primary system water. With the exception of one data point for the Alloy 600 specimen, the experimental results in water were bounded by the ANL model prediction and the "air line" for austenitic SSs from the ASME Code Section XI correlation.

Several CGR tests were performed on this set of specimens in HP water that contained ≈6 ppm DO at load ratios between 0.2 and 1.0. The CGRs in this environment were also compared with ANL model predictions for crack growth in oxygenated water and the air line from the ASME Section XI correlation at the K_{max} and load ratio values for the specimens. Once again, the experimental data were bounded by the two curves and the ANL model provides a good "upper-bound" estimate of the CGRs at all load ratios.

The morphology of corrosion-fatigue cracks in the Alloy 600 and austenitic SS specimens was determined. In simulated BWR water that contained ≈200 ppb DO, the crack path in the sensitized Type 304 SS specimens was predominantly intergranular. The Alloy 600 specimen, which has a very small grain size, also exhibited intergranular cracking in this environment. The crack path in the Alloy 600, Type 316NG and sensitized 304 SS specimens in which the environment at the beginning and end of the experiment was simulated PWR primary system water, with an intermediate period of oxygenated HP water, revealed transgranular cracking. Intergránular cracking of the sensitized Type 304 SS specimen in oxygenated water was not observed because of the low load ratio in most of the tests.

5.3 Irradiation-Assisted SCC of Type 304 SS

Effects of DO and electrochemical potential (ECP) on susceptibility of commercial-purity (CP) Type 304 SS BWR neutron-absorber tubes to IASCC, determined from slow-strain-rate tensile (SSRT) tests in simulated BWR water at 289°C, were similar to those of other CP-grade Type 304 SS BWR components reported by investigators. The threshold ECP and DO to protect the CP-grade materials against susceptibility to IASCC appear to be <-140 mV SHE and <0.01 ppm, respectively. For a fluence >1.3 x 10^{21} $n \cdot cm^{-2}$, susceptibility to IASCC seems to be determined primarily by DO or ECP, indicating a predominant effect of water chemistry and a secondary effect of fluence.

Dependence of IASCC susceptibility of specimens from BWR components fabricated from HP heats of Type 304 SS differed from those of the tubes fabricated from CP materials. In comparison to the latter materials, susceptibility of the former was less dependent on water chemistry (DO and ECP) and was significantly higher regardless of water chemistry and fluence.

The HP-grade neutron-absorber tubes were characterized by more pronounced grain-boundary Cr depletion and a higher level of fluorine contamination than the CP-grade absorber tubes or control-blade sheath. The behavior of HP neutron-absorber tubes can be explained by a model based on a catalytic role of fluorine ions on corrosion at the crack tip, coupled with grain-boundary Cr depletion in the material. In the model, corrosion of fluorine-contaminated grain boundaries is accelerated because the rate of formation of a ligand complex $FeF(H_2O)_5$ is orders-of-magnitude greater than the rate to form a fluorine-free complex $Fe(H_2O)_6$. The fluorine atom is released from the labile complex $FeF(H_2O)_5$ dissolved in water when H_2O replaces the fluorine atom, thus leading to a classical catalysis by fluorine. This catalytic reaction chain is broken when the concentration of Cr ions in water is high (e.g., near Cr-rich grain boundaries), because a $CrF(H_2O)_5$ complex forms rapidly but remains inert in water.

Intergranular crack growth rates estimated from our SSRT tests and constant-load tests conducted on specimens from BWR components at several laboratories are similar, but significantly higher than those estimated from the SSRT data reported for BWR-irradiated test specimens. At present, the origin of the discrepancy is not clear, although we suspect that differences in stress intensity and strain rate are the most likely reasons.

Nearly all components of a hot-cell J-R test facility have been fabricated and installed. The electronic control system has been connected and tested by technical support personnel from the Instron Corporation, Inc. The position LVDT has also been calibrated by Instron, and the load cell is being calibrated with the use of a standard. Work is in progress to align the load train and develop a LabVIEW™ data acquisition program.

References

1. K. Iida, *A Review of Fatigue Failures in LWR Plants in Japan*, Nucl. Eng. Des. **138**, 297–312 (1992).

2. *ASME Boiler and Pressure Vessel Code Section III – Rules for Construction of Nuclear Power Plant Components*, The American Society of Mechanical Engineers, 345 East 47th Street, New York, NY 10017, 1992 Edition.

3. D. A. Hale, S. A. Wilson, E. Kiss, and A. J. Gianuzzi, *Low Cycle Fatigue Evaluation of Primary Piping Materials in a BWR Environment*, GEAP–20244, U.S. Nuclear Regulatory Commission (Sept. 1977).

4. D. A. Hale, S. A. Wilson, J. N. Kass, and E. Kiss, *Low Cycle Fatigue Behavior of Commercial Piping Materials in a BWR Environment*, J. Eng. Mater. Technol. **103**, 15–25 (1981).

5. S. Ranganath, J. N. Kass, and J. D. Heald, *Fatigue Behavior of Carbon Steel Components in High-Temperature Water Environments*, in Low-Cycle Fatigue and Life Prediction, ASTM STP 770, C. Amzallag, B. N. Leis, and P. Rabbe, eds., American Society for Testing and Materials, Philadelphia, PA, pp. 436–459 (1982).

6. S. Ranganath, J. N. Kass, and J. D. Heald, *Fatigue Behavior of Carbon Steel Components in High-Temperature Water Environments*, in BWR Environmental Cracking Margins for Carbon Steel Piping, EPRI NP–2406, Electric Power Research Institute, Palo Alto, CA, Appendix 3 (May 1982).

7. J. B. Terrell, *Fatigue Life Characterization of Smooth and Notched Piping Steel Specimens in 288°C Air Environments*, NUREG/CR–5013, EM–2232 Materials Engineering Associates, Inc., Lanham, MD (May 1988).

8. J. B. Terrell, *Fatigue Strength of Smooth and Notched Specimens of ASME SA 106–B Steel in PWR Environments*, NUREG/CR–5136, MEA–2289, Materials Engineering Associates, Inc., Lanham, MD (Sept. 1988).

9. P. D. Hicks, in *Environmentally Assisted Cracking in Light Water Reactors: Semiannual Report October 1990—March 1991*, NUREG/CR–4667 Vol. 12, ANL–91/24, pp. 3–18 (Aug. 1991).

10. P. D. Hicks and W. J. Shack, in *Environmentally Assisted Cracking in Light Water Reactors, Semiannual Report, April–September 1991*, NUREG/CR–4667 Vol. 13, ANL–92/6, pp. 3–8 (March 1992).

11. O. K. Chopra, W. F. Michaud, and W. J. Shack, in *Environmentally Assisted Cracking in Light Water Reactors, Semiannual Report, October 1992–March 1993*, NUREG/CR–4667 Vol. 16, ANL–93/27, pp. 3–19 (Sept. 1993).

12. O. K. Chopra, W. F. Michaud, W. J. Shack, and W. K. Soppet, in *Environmentally Assisted Cracking in Light Water Reactors, Semiannual Report, April–September 1993*, NUREG/CR–4667 Vol. 17, ANL–94/16, pp. 1–22 (June 1994).

13. O. K. Chopra, W. F. Michaud, and W. J. Shack, in *Environmentally Assisted Cracking in Light Water Reactors, Semiannual Report, October 1993--March 1994*, NUREG/CR-4667 Vol. 18, ANL-95/2, pp. 3-10 (March 1995).

14. M. Higuchi and K. Iida, *Fatigue Strength Correction Factors for Carbon and Low-Alloy Steels in Oxygen-Containing High-Temperature Water*, Nucl. Eng. Des. **129**, 293-306 (1991).

15. K. Iida, H. Kobayashi, and M. Higuchi, *Predictive Method of Low Cycle Fatigue Life of Carbon and Low Alloy Steels in High Temperature Water Environments*, NUREG/CP-0067, MEA-2090, Vol. 2, Materials Engineering Associates, Inc., Lanham, MD (April 1986).

16. N. Nagata, S. Sato, and Y. Katada, *Low-Cycle Fatigue Behavior of Low-Alloy Steels in High-Temperature Pressurized Water*, in Transactions of 10th International Conf. on Structural Mechanics in Reactor Technology, F. A. H. Hadjian, ed., American Association for Structural Mechanics in Reactor Technology, Anaheim, CA (1989).

17. S. Majumdar, O. K. Chopra, and W. J. Shack, *Interim Fatigue Design Curves for Carbon, Low-Alloy, and Austenitic Stainless Steels in LWR Environments*, NUREG/CR-5999, ANL-93/3 (April 1993).

18. J. Keisler, O. K. Chopra, and W. J. Shack, *Statistical Analysis of Fatigue Strain-Life Data for Carbon and Low-Alloy Steels*, NUREG/CR-6237, ANL-94/21 (Aug. 1994).

19. L. A. James, *The Effect of Temperature and Cyclic Frequency Upon Fatigue Crack Growth Behavior of Several Steels in an Elevated Temperature Aqueous Environment*, J. Pressure Vessel Technol. **116**, 122-127 (1994).

20. T. A. Prater and L. F. Coffin, *The Use of Notched Compact-Type Specimens for Crack Initiation Design Rules in High-Temperature Water Environments*, in Corrosion Fatigue: Mechanics Metallurgy, Electrochemistry, and Engineering, ASTM STP 801, T. W. Crooker and B. N. Leis, eds., American Society for Testing and Materials, Philadelphia, PA, pp. 423-444 (1983).

21. T. A. Prater and L. F. Coffin, *Notch Fatigue Crack Initiation in High Temperature Water Environments: Experiments and Life Prediction*, J. of Pressure Vessel Technol., Trans. ASME, **109**, 124-134 (1987).

22. M. O. Speidel and R. M. Magdowski, *Stress Corrosion Cracking of Nuclear Reactor Pressure Vessel Steel in Water: Crack Initiation versus Crack Growth*, Corrosion 88, Paper No. 283, St. Louis, MO (March 1988).

23. F. P. Ford and P. L. Andresen, *Stress Corrosion Cracking of Low-Alloy Pressure Vessel Steel in 288°C Water*, in Proc. 3rd Int. Atomic Energy Agency Specialists' Meeting on Subcritical Crack Growth, NUREG/CP-0112, Vol. 1, pp. 37-56 (Aug. 1990).

24. P. M. Scott and D. R. Tice, *Stress Corrosion in Low-Alloy Steels*, Nucl. Eng. Des. **119**, 399-413 (1990).

25. W. H. Cullen, *The Effects of Sulfur Chemistry and Load Ratio on Fatigue Crack Growth Rates in LWR Environments*, in Proc. 2nd Int. Atomic Energy Agency Specialists' Meeting on Subcritical Crack Growth, NUREG/CP-0067, MEA-2090, Vol. 2, pp. 339-355 (April 1986).

26. J. D. Atkinson, J. H. Bulloch, and J. E. Forrest, *TA Fractographic Study of Fatigue Cracks Produced in A533B Pressure Vessel Steel Exposed to Simulated PWR Primary Water Environments*, in Proc. 2nd Int. Atomic Energy Agency Specialists' Meeting on Subcritical Crack Growth, NUREG/CP-0067, MEA-2090, Vol. 2, pp. 269-290 (April 1986).

27. W. A. Van Der Sluys and D. S. DeMiglio, *An Investigation of Fatigue Crack Growth in SA508-2 in a 288°C PWR Environment by a Constant ΔK Test Method*, in Proc. Int. Atomic Energy Agency Specialists' Meeting on Subcritical Crack Growth, NUREG/CP-0044, MEA-2014, Vol. 1, pp. 44-64 (May 1983).

28. J. H. Bulloch, *A Review of the Fatigue Crack Extension Behavior of Ferritic Pressure Vessel Materials in Pressurized Water Reactor Environments*, Res. Mechanica, **26**, 95-172 (1989).

29. T. F. Kassner, W. J. Shack, W. E. Ruther, and J. H. Park, *Environmentally Assisted Cracking of Ferritic Steels*, in Environmentally Assisted Cracking in Light Water Reactors: Semiannual Report, April-September 1990, NUREG/CR-4667, Vol. 11, ANL-91/9, pp. 2-9 (May 1991).

30. D. D. Macdonald, S. Smialowska, and S. Pednekar, *The General and Localized Corrosion of Carbon and Low-Alloy Steels in Oxygenated High-Temperature Water*, NP-2853 (Feb. 1983).

31. J. Kuniya, H. Anzai, and I. Masaoka, *Effect of MnS Inclusions on Stress Corrosion Cracking in Low-Alloy Steels*, Corrosion, **48** (5), 419-425 (1992).

32. F. P. Ford, S. Ranganath, and D. Weinstein, *Environmentally Assisted Fatigue Crack Initiation in Low-Alloy Steels - A Review of the Literature and the ASME Code Design Requirements*, EPRI Report TR-102765 (Aug. 1993).

33. W. J. Shack and T. F. Kassner, *Review of Environmental Effects on Fatigue Crack Growth of Austenitic Stainless Steels*, NUREG/CR-6176, ANL-94/1, (May 1994).

34. W. E. Ruther, T. F. Kassner, and J. Y. Park, in *Environmentally Assisted Cracking in Light Water Reactors, Semiannual Report, October 1991-March 1992*, NUREG/CR-4667 Vol. 14, ANL-92/30, pp. 33-45 (Aug. 1992).

35. W. E. Ruther and T. F. Kassner, in *Environmentally Assisted Cracking in Light Water Reactors, Semiannual Report, April-September 1993*, NUREG/CR-4667 Vol. 17, ANL-94/16, pp. 22-34 (June 1994).

36. P. L. Andresen and F. P. Ford, "*Irradiation Assisted Stress Corrosion Cracking: From Modeling and Prediction of Laboratory and In-Core Response to Component Life Prediction*, Corrosion 95, Paper No. 419, Orlando, FL (March 1995).

37. M. E. Indig, J. L. Nelson, and G. P. Wozadlo, *Investigation of the Protection Potential Against IASCC*, Proc. 5th Int. Symp. Environmental Degradation of Materials in Nuclear Power Systems - Water Reactors, D. Cubicciotti, E. P. Simonen, and R. Gold, eds., American Nuclear Society, La Grange Park, IL, pp. 941-947 (1992).

38. M. Kodama, S. Nishimura, J. Morisawa, S. Shima, S. Suzuki, and M. Yamamoto, *Effects of Fluence and Dissolved Oxygen on IASCC in Austenitic Stainless Steels,* Proc. 5th Int. Symp. on Environmental Degradation of Materials in Nuclear Power Systems – Water Reactors, D. Cubicciotti, E. P. Simonen, and R. Gold, eds., American Nuclear Society, La Grange Park, IL, pp. 948-954 (1992).

39. M. Kodama, R. Katsura, J. Morisawa, S. Nishimura, S. Suzuki, K. Asano, K. Fukuya, and K. Nakata, *IASCC Susceptibility of Austenitic Stainless Steels Irradiated to High Neutron Fluence,* Proc. 6th Int. Symp. on Environmental Degradation of Materials in Nuclear Power Systems - Water Reactors, R. E. Gold and E. P. Simonen, eds., The Minerals, Metals, and Materials Society, Warrendale, PA, pp. 583–588 (1993).

40. R. Katsura, J. Morisawa, M. Kodama, S. Nishimura, S. Suzuki, S. Shima, and M. Yamamoto, *Effect of Stress on IASCC in Irradiated Austenitic Stainless Steels,* Proc. 6th Int. Symp. on Environmental Degradation of Materials in Nuclear Power Systems - Water Reactors, R. E. Gold and E. P. Simonen, eds., The Minerals, Metals, and Materials Society, Warrendale, PA, pp. 625–631 (1993).

41. A. Jenssen and L. G. Ljungberg, *Irradiation Assisted Stress Corrosion Cracking of Stainless Steel Alloys in BWR Normal Water Chemistry and Hydrogen Water Chemistry,* Proc. 6th Int. Symp. on Environmental Degradation of Materials in Nuclear Power Systems - Water Reactors, R. E. Gold and E. P. Simonen, eds., The Minerals, Metals, and Materials Society, Warrendale, PA, pp. 547–553 (1993).

42. H. M. Chung, W. E. Ruther, J. E. Sanecki, A. G. Hins, and T. F. Kassner, *Stress Corrosion Cracking Susceptibility of Irradiated Type 304 Stainless Steels,* Effects of Radiation on Materials: Proc. 16th Int. Symp., ASTM STP 1175, A. S. Kumar, D. S. Gelles, R. K. Nanstad, and T. A. Little, eds., American Society for Testing and Materials, Philadelphia, pp. 851–869 (1993).

43. H. M. Chung, W. E. Ruther, J. E. Sanecki, and T. F. Kassner, *Grain-Boundary Microchemistry and Intergranular Cracking of Irradiated Austenitic Stainless Steel,* Proc. 6th Int. Symp. on Environmental Degradation of Materials in Nuclear Power Systems - Water Reactors, R. E. Gold and E. P. Simonen, eds., The Minerals, Metals, and Materials Society, Warrendale, PA, pp. 511–519 (1993).

44. A. J. Jacobs, G. P. Wozadlo, K. Nakata, T. Yoshida, and I. Masaoka, *Radiation Effects on the Stress Corrosion and Other Selected Properties of Type 304 and Type 316 Stainless Steels,* Proc. 3rd Int. Symp. on Environmental Degradation of Materials in Nuclear Power Systems – Water Reactors, G. J. Theus and J. R. Weeks, eds., The Metallurgical Society, Warrendale, PA, pp. 673–681 (1988).

45. H. M. Chung, W. E. Ruther, and J. E. Sanecki, in *Environmentally Assisted Cracking in Light Water Reactors: Semiannual Report, October 1993–March 1994,* NUREG/CR–4667 Vol. 18, ANL–95/2, pp. 27–35 (March 1995).

46. C. T. Ward, D. L. Mathis, and R. W. Staehle, *Intergranular Attack of Sensitized Austenitic Stainless Steel by Water Containing Fluoride Ions,* Corrosion **25,** 394–396 (1969).

47. N. C. Huang and Z. Nagy, *Kinetics of the Ferrous/Ferric Electrode Reaction in the Absence of Chloride Catalysis,* J. Electrochem. Soc. **134**, 2215–2220 (1987).

Distribution for NUREG/CR-4667, Vol. 19 (ANL-95/25)

Internal

W. J. Shack (45)

TIS Files

External

NRC, for distribution per R5

Libraries

ANL–E (2)

ANL–W

Manager, Chicago Field Office, DOE

Energy Technology Division Review Committee:

H. K. Birnbaum, University of Illinois, Urbana

R. C. Buchanan, University of Cincinnati, Cincinnati, OH

M. S. Dresselhaus, Massachusetts Institute of Technology, Cambridge, MA

B. G. Jones, University of Illinois, Urbana

C.–Y. Li, Cornell University, Ithaca, NY

S. N. Liu, Fremont, CA

R. E. Smith, Altran Corporation, Huntersville, NC

P. L. Andresen, General Electric Corporate Research and Development, Schenectady, NY

T. A. Auten, Knolls Atomic Power Laboratory

R. G. Ballinger, Massachusetts Institute of Technology, Cambridge, MA

W. H. Bamford, Structural Materials Engineering, Westinghouse Electric Corp., Pittsburgh

S. M. Bruemmer, Battelle Pacific Northwest Laboratory

H. S. Chung, Korea Atomic Energy Research Institute, Daejeon, Korea

L. Coressti, ABB CE Nuclear Power, Windsor, CT

R. L. Cowan, General Electric Co., San Jose, CA

G. Cragnolino, Southwest Research Inst., San Antonio, TX

W. H. Cullen, Materials Engineering Assoc., Inc., Lanham, MD

E. D. Eason, Modeling and Computing Services, Newark, CA

M. Fox, Tucson, AZ

D. G. Franklin, Bettis Atomic Power Laboratory

Y. S. Garud, S. Levy, Inc., Campbell, CA

F. Garzarolli, KWU, Erlangen, Germany

J. Gilman, Electric Power Research Inst., Palo Alto, CA

B. M. Gordon, General Electric Co., San Jose, CA

M. M. Hall, Bettis Atomic Power Laboratory

J. W. Halley, U. Minnesota, Minneapolis

H. E. Hanninen, Technical Research Centre of Finland, Espoo

D. Harrison, USDOE, Germantown, MD

J. Hickling, CML Capcis March Ltd., Erlangen-Tennonlohe, Germany

M. Higuchi, Ishikawajima–Harima Heavy Industries Co., Ltd., Japan

C. Hoffmann, ABB CE Nuclear Power, Windsor, CT

H. S. Isaacs, Brookhaven National Laboratory

A. Jacobs, General Electric Co., San Jose, CA

L. James, Bettis Atomic Power Laboratory

C. Jansson, Vattenfall Energisystem, Vallingby, Sweden

D. P. Jones, Bettis Atomic Power Laboratory

R. H. Jones, Battelle Pacific Northwest Laboratory

R. L. Jones, Electric Power Research Institute, Palo Alto, CA

T. Karlsen, OECD Halden Reactor Project, Halden, Norway

C. Kim, Westinghouse Electric Corp., Pittsburgh

L. Ljungberg, ASEA-ATOM, Vasteras, Sweden

C. D. Lundin, U. Tennessee, Knoxville

D. D. Macdonald, Pennsylvania State University, University Park

T. R. Mager, Westinghouse Electric Corp., Pittsburgh

R. D. McCright, Lawrence Livermore National Laboratory

A. R. McIlree, Electric Power Research Institute, Palo Alto, CA

H. Metha, General Electric Co., San Jose, CA

D. Morgan, Pennsylvania Power and Light Co., Allentown, PA

J. L. Nelson, Electric Power Research Inst., Palo Alto, CA

D. H. Njo, Swiss Federal Nuclear Safety Inspectorate, Villigen, Switzerland

M. Pytel, Structural Integrity Associates, San Jose, CA

M. Prager, Materials Properties Council, New York, NY

S. Ranganath, General Electric Co., San Jose, CA

P. M. Scott, Framatome, Paris, France

J. Sedriks, Office of Naval Research, Arlington, VA

C. Shepherd, AEA Technology–Harwell Labs., Didcot, Oxon, UK

S. Smialowska, Ohio State University, Columbus

H. D. Solomon, General Electric Corporate Research and Development, Schenectady, NY

M. O. Speidel, Swiss Federal Institute of Technology, Zurich, Switzerland

D. M. Stevens, Lynchburg Research Center, Babcock & Wilcox Co., Lynchburg, VA

W. A. Van Der Sluys, Research & Development Division, Babcock & Wilcox Co., Alliance, OH

J. C. Van Duysen, Electricite de France-Research and Development Centre de Renardieres, Moret–sur–Loing, France

E. Venerus, Knolls Atomic Power Laboratory

C. Vitanza, OECD Halden Reactor Project, Halden, Norway

G. S. Was, University of Michigan, Ann Arbor

J. R. Weeks, Brookhaven National Laboratory

D. Winkel, Teleco Oil Field Services, Meriden, CT

S. Yukawa, Boulder, CO

NRC FORM 335 (2–89) NRCM 1102, 3201, 3202

U. S. NUCLEAR REGULATORY COMMISSION

BIBLIOGRAPHIC DATA SHEET

(See instructions on the reverse)

1. REPORT NUMBER *(Assigned by NRC. Add Vol., Supp., Rev., and Addendum Numbers, if any.)*
NUREG/CR–4667, Vol. 19
ANL–95/25

2. TITLE AND SUBTITLE
Environmentally Assisted Cracking in Light Water Reactors.
Semiannual Report April 1994—September 1994

3. DATE REPORT PUBLISHED

MONTH	YEAR
September	1995

4. FIN OR GRANT NUMBER
A2212

5. AUTHOR(S)
O. K. Chopra, H. M. Chung, D. J. Gavenda, E. E. Gruber, A. G. Hins, T. H. Hughes, T. F. Kassner, W. E. Ruther, W. J. Shack, and W. K. Soppet

6. TYPE OF REPORT
Technical; Semiannual

7. PERIOD COVERED *(Inclusive Dates)*
April 1994—September 1994

8. PERFORMING ORGANIZATION – NAME AND ADDRESS *(If NRC, provide Division, Office or Region, U.S. Nuclear Regulatory Commission, and mailing address; if contractor, provide name and mailing address.)*

Argonne National Laboratory
9700 South Cass Avenue
Argonne, IL 60439

9. SPONSORING ORGANIZATION – NAME AND ADDRESS *(If NRC, type "Same as above": if contractor, provide NRC Division, Office or Region, U.S. Nuclear Regulatory Commission, and mailing address.)*

Division of Engineering
Office of Nuclear Regulatory Research
U. S. Nuclear Regulatory Commission
Washington, DC 20555–0001

10. SUPPLEMENTARY NOTES

M. McNeil, NRC Project Manager

11. ABSTRACT (200 words or less)

This report summarizes work performed by Argonne National Laboratory (ANL) on fatigue and environmentally assisted cracking (EAC) in light water reactors from April to September 1994. Topics that have been investigated include (a) fatigue of carbon and low–alloy steel used in piping and reactor pressure vessels, (b) EAC of austenitic stainless steels (SSs) and Alloy 600, and (c) irradiation–assisted stress corrosion cracking (IASCC) of Type 304 SS. Fatigue tests have been conducted on A106–Gr B and A533–Gr B steels in oxygenated water to determine whether a slow strain rate applied during different portions of a tensile–loading cycle are equally effective in decreasing fatigue life. Crack growth data were obtained on fracture–mechanics specimens of SSs and Alloy 600 to investigate EAC in simulated boiling water reactor (BWR) and pressurized water reactor environments at 289°C. The data were compared with predictions from crack growth correlations developed at ANL for SSs in water and from rates in air from Section XI of the ASME Code. Microchemical changes in high– and commercial–purity Type 304 SS specimens from control–blade absorber tubes and a control–blade sheath from operating BWRs were studied by Auger electron spectroscopy and scanning electron microscopy to determine whether trace impurity elements may contribute to IASCC of these materials.

12. KEY WORDS/DESCRIPTORS *(List words or phrases that will assist researchers in locating this report.)*
Corrosion Fatigue
Crack Growth
Irradiation–Assisted Stress Corrosion Cracking
Radiation–Induced Segregation
Stress Corrosion Cracking
A106–Gr B Steel
A302–Gr B Steel
A533–Gr B Steel
Alloy 600
Types 316NG and 304 Stainless Steel

13. AVAILABILITY STATEMENT
Unlimited

14. SECURITY CLASSIFICATION
(This Page)
Unclassified
(This Report)
Unclassified

15. NUMBER OF PAGES

16. PRICE

NRC FORM 335 (2–89)